AIAA JOURNAL
Vol. 41, No. 5, May 2003

Efficient and Robust Reynolds-Stress Model Computation of Three-Dimensional Compressible Flows

J. C. Chassaing,* G. A. Gerolymos,† and I. Vallet‡
Université Pierre-et-Marie-Curie, 91405 Paris, France

The purpose of this work is the development of an efficient and robust implicit methodology for the integration of the three-dimensional compressible Favre–Reynolds-averaged Navier–Stokes equations with near-wall Reynolds-stress closure. The five mean-flow and seven turbulence transport equations are discretized in space, on a structured multiblock grid, using an $\mathcal{O}(\Delta x^3)$ finite volume upwind-biased MUSCL scheme with Van Leer flux vector splitting and Van Albada limiters. Time integration is based on an implicit dual-time-stepping procedure with alternating direction implicit subiterations. A particular treatment of the approximate Jacobians used in the subiterations substantially diminishes the computing time requirements of the implicit phase, so that the computational overhead of the Reynolds-stress seven-equation closure, compared to a two-equation closure, is less than 30% per iteration. For steady flow computations local time steps are used, for both the subiterations and the time marching, with Courant–Friedrichs–Lewy numbers of $\mathcal{O}(10–20)$ for the $\mathcal{O}(1–20)$ subiterations needed and $\mathcal{O}(100–500)$ for the time marching. The robustness of the method is ensured by appropriate positivity, boundedness, and Reynolds-stress realizability constraints. The numerical method is illustrated by computing (and conducting numerical studies) for a high subsonic ($M \sim 0.7$) three-dimensional flow with large separation and for a transonic three-dimensional shock-wave/boundary-layer interaction.

Introduction

NUMEROUS authors have justified the use of simple zero-equation closures[1] or the development of such ad hoc closures as transport equations for the eddy viscosity[2] (a quantity that cannot be defined theoretically) by stating that more advanced closures (two-equation or full Reynolds-stress) require too much computer resources and, more importantly, are numerically unstable.[2] As far as two-equation closures are concerned, these arguments have been brushed away by the widespread use of such closures.[3–5] Indeed careful implementation of two-equation closures yields quite robust and computationally efficient methods,[6–9] and this has established two-equation closures as the current standard in turbulence modeling. What is surprising is that these same arguments of computational cost and numerical instability are being currently employed by developers of explicit algebraic Reynolds-stress models[10] against the use of full Reynolds-stress models (RSM).[4,5] These assertions are of course negated by the increasing number of three-dimensional near-wall RSM computations reported in the literature.[11–16]

There are, however, only a few published papers concerned with the numerical implementation of full near-wall Reynolds-stress models for three-dimensional compressible flows with shock waves, such as those encountered in aerospace applications (Table 1)[8,12,14,15,17–37]:

1) The structured multiblock cell-centered finite volume method developed by Morrison[17] (Table 1) has been applied to the computation of Mach $M = 2.87$ compression ramps[38] (with angles of 8, 16, and 20 deg) and of two-dimensional[39] and three-dimensional[13] supersonic ($M = 1.8$) injection at 25 deg in a supersonic ($M = 3$) crossflow. No detailed information on iterative convergence is given, although it is stated by Chenault et al.[13] that for the three-dimensional computations the L_2 norm of the residuals was reduced by three orders of magnitude, before saturation. No information on time-step choice or on realizability[31] constraints implementation is available.[13,17,38,39]

2) The structured multiblock cell-vertex finite volume method developed by Vallet[21] (Table 1) has been applied to the computation of two-dimensional[12,15,21] and three-dimensional[12,15] shock-wave/boundary-layer interactions and of complex transonic three-dimensional flows in turbomachinery.[16] For attached flows and for flows with small separation, computations were performed at Courant–Friedrichs–Lewy (CFL) = von Neumann number (VNN) = 20–50. For flows with extended separation, it was often necessary to reduce the VNN number (CFL = 20, VNN = 2). Convergence of the L_2 norm of the residuals saturated after a reduction of four orders of magnitude.[21] Explicit application of realizability constraints[12,15] was found to be the cornerstone of the stability of the method and resulted in a very robust solver.

3) The structured cell-centered finite volume method developed by Batten et al.[8] (Table 1) has been applied to the computation of two-dimensional and axisymmetric shock-wave/boundary-layer interactions and of the three-dimensional flowfield around a fin/plate junction in a supersonic ($M = 2$) flow. For the three-dimensional computations[14] the CFL was raised progressively from 1 to 1000, and residuals were reduced by three orders of magnitude, without reaching saturation. (Further iterations might be necessary for full convergence of the turbulence quantities.)

All of these methods are upwind and strongly implicit. The implicit phase induces a substantial overhead (factor 3–4) compared to two-equation closures (e.g., 12×12 blocks for the method of Morrison[17] or $1 + 2 \times 23$ bandwidth for the method of Vallet[21] compared to 7×7 and $1 + 2 \times 13$ for two-equation closures).

The purpose of the present paper is to develop an efficient and robust method for the computation of the compressible Navier–Stokes equations with RSM closure. (The choice of an upwind implicit method is an obvious one, based on the review of the literature.) The basic improvements of the new method are as follows:

1) One improvement is the use of a dual-time-stepping (DTS) technique, analogous to the one used for unsteady flows,[40] but with local time steps for both the time advancement and the subiterations, an original combination that will be here called local-dual-time-stepping technique (LDTS), which enhances convergence and solution quality (through reduction of the factorization error), and is able to resolve limit-cycle-oscillation problems observed, for flows

Received 22 June 2002; revision received 23 November 2002; accepted for publication 30 November 2002.

*Research Engineer, Laboratoire d'Energétique, Unité Mixte de Recherche du Centre National de Recherche Scientifique, Building 511, Orsay.
†Professor, Director, Laboratoire d'Energétique, Building 511, Orsay; geg@ccr.jussieu.fr.
‡Assistant Professor, Laboratoire d'Energétique, Unité Mixte de Recherche du Centre National de Recherche Scientifique, Building 511, Orsay.

Table 1 Computational methods with near-wall RSMs applied to three-dimensional transonic flows

Characteristic	Morrison[17]	Vallet[18]	Batten et al.[8]
Year	1992	1995	1997
RSM	ZSGS[19a]	LSS,[12b] GV,[15c] GSV-LSS[20d]	MCL[14e]
$\underline{F}_\ell^C$[f]	$\mathcal{O}(\Delta x^2)$ MUSCL[21] upwind Roe[22,23] scheme with minmod[22,23] or Venkatakrishnan[24] limiters	$\mathcal{O}(\Delta x^3)$ MUSCL[21] upwind-biased Van Leer[21] with κ-scheme Van Albada limiter[21,25]	$\mathcal{O}(\Delta x^2)$ MUSCL[21] upwind HLLC approximate Riemann solver[22] with various limiters[8]
$\underline{F}_\ell^V$, $\underline{S}$[g]	$\mathcal{O}(\Delta x^2)$ centered[26]	$\mathcal{O}(\Delta x^2)$ centered[26]	$\mathcal{O}(\Delta x^2)$ centered[26]
Time	$\mathcal{O}(\Delta t)$ ADI–AF[21h] 12×12 block tridiagonal	$\mathcal{O}(\Delta t)$ ADI–AF[21] banded-LU factorization[27] with bandwidth $1 + 2 \times 23$	$\mathcal{O}(\Delta t)$ line relaxation[28] with three alternate sweeps with explicit deferred corrections[14]
$\underline{F}^J$[i]	$\mathcal{O}(\Delta x)$ conservative[28] stencil implicit AF source-terms	$\mathcal{O}(\Delta x)$ conservative[28] stencil explicit source terms	$\mathcal{O}(\Delta x)$ conservative[28] stencil diagonalized RSM Jacobians apparent viscosity technique[29,30]
bc[j]	——	Implicit Chakravarthy[23]	Implicit Chakravarthy[23]
Realizability[31]	——	Explicit constraints[12,15]	Pantakar linearization,[8,32]
[CFL, VNN][k,l]	——	[20–50, 2–50]	[1–1000,1–1000]

[a]ZSGS: Zhang–So–Gatski–Speziale.[19]
[b]LSS: Launder–Shima[33] with Launder–Sharma[34] ε^*-equation.
[c]GV: Gerolymos–Vallet.[15]
[d]GSV-LSS: Gerolymos–Sauret–Vallet[20] wall-normal free version of the LSS model.
[e]MCL: modified[14] Craft–Launder.[35]
[f]$\underline{F}_\ell^C$: discretization of convective fluxes.
[g]$\underline{F}_\ell^V$, $\underline{S}$: discretization of viscous fluxes and of the gradients appearing in viscous, diffusive, and source terms.
[h]ADI–AF: alternative-directions-implicit-approximate factorization.
[i]$\underline{F}^J$: approximate Jacobians used in the implicit phase.
[j]bc: boundary conditions.
[k]CFL: convective stability[36,37] Courant–Friedrichs–Lewy number.
[l]VNN: convective stability[36,37] von Neumann number.

with large separation, using standard alternating-direction-implicit (ADI)–approximate-factorization (AF) techniques.

2) Another improvement is the introduction of an appropriate approximation of the implicit matrices, which minimizes the computational cost of the turbulence transport equations, that is applicable to both two-equation and seven-equation (RSM) closures and substantially improves computational efficiency.

Flow Model and Computational Method

Flow Model

The flow is modeled by the compressible Favre–Reynolds-averaged three-dimensional Navier–Stokes equations,[15] coupled to the six transport equations for the Reynolds stresses and the transport equation for the turbulence-kinetic-energy modified dissipation rate,[15] written symbolically as

$$\frac{\partial \underline{w}}{\partial t} + \frac{\partial \underline{F}_\ell}{\partial x_\ell} + \underline{S} \equiv \frac{\partial \underline{w}}{\partial t} + \frac{\partial \underline{F}_x}{\partial x} + \frac{\partial \underline{F}_y}{\partial y} + \frac{\partial \underline{F}_z}{\partial z} + \underline{S} = 0 \tag{1}$$

$$\underline{w} = \left[\bar{\rho}, \bar{\rho}\tilde{u}, \bar{\rho}\tilde{v}, \bar{\rho}\tilde{w}, \bar{\rho}\breve{h}_t - \bar{p}, \bar{\rho}\widetilde{u''u''}, \bar{\rho}\widetilde{u''v''}, \bar{\rho}\widetilde{v''v''}, \bar{\rho}\widetilde{v''w''}, \bar{\rho}\widetilde{w''w''}, \bar{\rho}\widetilde{w''u''}, \bar{\rho}\varepsilon^*\right]^T \in \mathbb{R}^{12} \tag{2}$$

$$\underline{F}_\ell = \underline{F}_\ell^C + \underline{F}_\ell^V$$

$$\underline{F}_\ell^C = \left[\bar{\rho}\tilde{u}_\ell, \bar{\rho}\tilde{u}_\ell\tilde{u} + \bar{p}\delta_{x\ell}, \bar{\rho}\tilde{u}_\ell\tilde{v} + \bar{p}\delta_{y\ell}, \bar{\rho}\tilde{u}_\ell\tilde{w} + \bar{p}\delta_{z\ell}, \bar{\rho}\tilde{u}_\ell\breve{h}_t, \bar{\rho}\tilde{u}_\ell\widetilde{u''u''}, \bar{\rho}\tilde{u}_\ell\widetilde{u''v''}, \bar{\rho}\tilde{u}_\ell\widetilde{v''v''}, \bar{\rho}\tilde{u}_\ell\widetilde{v''w''}, \bar{\rho}\tilde{u}_\ell\widetilde{w''w''}, \bar{\rho}\tilde{u}_\ell\widetilde{w''u''}, \bar{\rho}\tilde{u}_\ell\varepsilon^*\right]^T$$

$$\underline{F}_\ell^V = \left[0, \bar{\rho}\widetilde{u''_\ell u''} - \bar{\tau}_{\ell x}, \bar{\rho}\widetilde{u''_\ell v''} - \bar{\tau}_{\ell y}, \bar{\rho}\widetilde{u''_\ell w''} - \bar{\tau}_{\ell z}, \tilde{u}_i(\bar{\rho}\widetilde{u''_i u''_\ell} - \bar{\tau}_{i\ell}) + (\bar{q}_\ell + \bar{\rho}\widetilde{h''u''_\ell}), -\mathcal{D}_{xx\ell}, -\mathcal{D}_{xy\ell}, -\mathcal{D}_{yy\ell}, -\mathcal{D}_{yz\ell}, -\mathcal{D}_{zz\ell}, -\mathcal{D}_{zx\ell}, -\mathcal{D}_{\varepsilon_\ell}\right]^T \tag{3}$$

$$\underline{S} = -\left[0, 0, 0, 0, S_{\breve{h}_t}, S_{uu}, S_{uv}, S_{vv}, S_{vw}, S_{ww}, S_{wu}, S_\varepsilon\right]^T \tag{4}$$

where $\underline{w} \in \mathbb{R}^{12}$ is the vector of unknowns; $\underline{F}_\ell \in \mathbb{R}^{12}$ ($\underline{F}_x$, $\underline{F}_y$, $\underline{F}_z$) are the combined convective ($\underline{F}_\ell^C$) and diffusive (viscous; $\underline{F}_\ell^V$) fluxes; $\underline{S} \in \mathbb{R}^{12}$ are the source terms; t is the time; x_ℓ (x, y, z) are the Cartesian space coordinates; u_i (u, v, w) are the velocity components; ρ is the density; p is the pressure; δ_{ij} is the Kronecker symbol; τ_{ij} are the viscous stresses, q_i are the molecular heat fluxes; $\mathcal{D}_{ijk}$ represents the order three tensor responsible for the turbulent diffusion of the Reynolds stresses $d_{ij} = \partial \mathcal{D}_{ij\ell}/\partial x_\ell$ (including triple correlations, pressure diffusion, and viscous diffusion); and $\mathcal{D}_{\varepsilon_\ell}$ corresponds to the diffusion of the turbulence-kinetic-energy dissipation rate ε. The symbol $(\tilde{\cdot})$ indicates Favre averaging, $(\bar{\cdot})$ nonweighted averaging, $(\cdot'')$ Favre fluctuations, and $(\cdot')$ nonweighted fluctuations. Also, $\breve{h}_t = \tilde{h} + \frac{1}{2}\tilde{u}_i\tilde{u}_i$ is the total enthalpy of the mean flow, h is the specific enthalpy, $k = \frac{1}{2}\widetilde{u''_i u''_i}$ is the turbulence kinetic energy. The symbol $(\breve{\cdot})$ is used to denote a function of average quantities that is neither a Favre average nor a nonweighted average. Finally $S_{\breve{h}_t}$ is the source term in the mean-flow energy equation[15] $S_{u_i u_j} = P_{ij} + \phi_{ij} - \bar{\rho}\varepsilon_{ij} + K_{ij} + \frac{2}{3}\phi_p\delta_{ij}$, P_{ij} is the production tensor, ϕ_{ij} is the redistribution tensor, ε_{ij} is the dissipation tensor, K_{ij} are direct compressibility effects,[15] ϕ_p is the pressure–dilatation correlation ($\overline{p'\partial u''_\ell/\partial x_\ell}$), and S_ε the source term in the ε equation.

The terms $\mathcal{D}_{ij\ell}$, ϕ_{ij}, ε_{ij}, K_{ij}, $\mathcal{D}_{\varepsilon_\ell}$, $S_{\breve{h}_t}$, S_ε, and $\widetilde{h''u''_\ell}$ depend on the particular closure used. In the computational examples reported in the present paper, two wall-normal-free RSM were used,[15,20] but the numerical implementation described in the following can be used with other closures (RSM or two equation).

Space Discretization

Equations (1) are discretized on a structured grid using a finite volume technique with vertex storage. The divergence of convective fluxes ($[F_x^C, F_y^C, F_z^C]^T \in \mathbb{R}^{12} \otimes \mathbb{E}^3$) is discretized using the flux-vector-splitting method of Van Leer with $\mathcal{O}(\Delta x^3)$ MUSCL interpolation and Van Albada limiters.[21,25] The divergence of viscous fluxes ($[\underline{F}_x^V, \underline{F}_y^V, \underline{F}_z^V]^T \in \mathbb{R}^{12} \otimes \mathbb{E}^3$) is discretized using the $\mathcal{O}(\Delta x^2)$ centered scheme described by Arnone.[26] The present implementation follows closely the work of Anderson et al.[21,25] Defining a staggered grid

$$x_{i\pm\frac{1}{2},j\pm\frac{1}{2},k\pm\frac{1}{2}} = \tfrac{1}{8}(x_{i,j,k} + x_{i\pm1,j,k} + x_{i\pm1,j\pm1,k} + x_{i,j\pm1,k} + x_{i,j,k\pm1} + x_{i\pm1,j,k\pm1} + x_{i\pm1,j\pm1,k\pm1} + x_{i,j\pm1,k\pm1}) \tag{5}$$

and noting (ξ, η, ζ) the grid directions (i, j, k), $({}^\xi\mathcal{S}_{i\pm1/2,j,k}$, ${}^\eta\mathcal{S}_{i,j\pm1/2,k}$, ${}^\zeta\mathcal{S}_{i,j,k\pm1/2})$ the cell-face areas of the staggered grid cell around the point (i, j, k), and $([{}^\xi n_x, {}^\xi n_y, {}^\xi n_z]^T_{i\pm1/2,j,k}$, $[{}^\eta n_x, {}^\eta n_y, {}^\eta n_z]^T_{i,j\pm1/2,k}$, $[{}^\zeta n_x, {}^\zeta n_y, {}^\zeta n_z]^T_{i,j,k\pm1/2})$ the corresponding unit normals

(positive in the positive grid direction), the semidiscrete scheme can be written as

$$\frac{\mathrm{d}\underline{w}_{i,j,k}}{\mathrm{d}t}+\frac{1}{\mathcal{V}_{i,j,k}}\begin{bmatrix}+{}^{\xi}\mathcal{S}_{i+\frac{1}{2},j,k}\ {}^{\xi}\underline{F}^{N}_{i+\frac{1}{2},j,k}-{}^{\xi}\mathcal{S}_{i-\frac{1}{2},j,k}\ {}^{\xi}\underline{F}^{N}_{i-\frac{1}{2},j,k}\\ +{}^{\eta}\mathcal{S}_{i,j+\frac{1}{2},k}\ {}^{\eta}\underline{F}^{N}_{i,j+\frac{1}{2},k}-{}^{\eta}\mathcal{S}_{i,j-\frac{1}{2},k}\ {}^{\eta}\underline{F}^{N}_{i,j-\frac{1}{2},k}\\ +{}^{\zeta}\mathcal{S}_{i,j,k+\frac{1}{2}}\ {}^{\zeta}\underline{F}^{N}_{i,j,k+\frac{1}{2}}-{}^{\zeta}\mathcal{S}_{i,j,k-\frac{1}{2}}\ {}^{\zeta}\underline{F}^{N}_{i,j,k-\frac{1}{2}}\end{bmatrix}+\underline{S}_{i,j,k}\cong 0 \tag{6}$$

where $\mathcal{V}_{i,j,k}$ is the control volume. The numerical flux is given by

$${}^{\xi}\underline{F}^{N}_{i\pm\frac{1}{2},j,k}=\Big[\underline{F}^{+}\big(\underline{w}^{-};{}^{\xi}n_x,{}^{\xi}n_y,{}^{\xi}n_z\big)+\underline{F}^{-}\big(\underline{w}^{+};{}^{\xi}n_x,{}^{\xi}n_y,{}^{\xi}n_z\big)+\underline{F}^{V}_{\ell}\,{}^{\xi}n_{\ell}\Big]_{i\pm\frac{1}{2},j,k} \tag{7}$$

The viscous fluxes at the staggered grid cell faces are given by

$$\Big[\underline{F}^{V}_{\ell}\Big]_{i\pm\frac{1}{2},j,k}=\tfrac{1}{2}\Big(\Big[\underline{F}^{V}_{\ell}\Big]_{i,j,k}+\Big[\underline{F}^{V}_{\ell}\Big]_{i\pm1,j,k}\Big) \tag{8}$$

and the Van Leer fluxes are given by

$$\underline{F}^{\pm}=\underbrace{\begin{bmatrix}0\\0\\0\\0\\0\\0\\0\\0\\0\\0\\0\\0\end{bmatrix}}_{\pm\check{M}_n<-1}+\underbrace{\pm\tilde{\rho}\check{a}\frac{(\check{M}_n\pm1)^2}{4}\begin{bmatrix}1\\ n_x\frac{\check{a}}{\gamma}(-\check{M}_n\pm2)+\tilde{u}\\ n_y\frac{\check{a}}{\gamma}(-\check{M}_n\pm2)+\tilde{v}\\ n_z\frac{\check{a}}{\gamma}(-\check{M}_n\pm2)+\tilde{w}\\ \frac{-(\gamma-1)\check{M}_n^2\pm2(\gamma-1)\check{M}_n+2}{\gamma^2-1}\check{a}^2+\frac{\tilde{V}^2}{2}\\ \widetilde{u''u''}\\ \widetilde{u''v''}\\ \widetilde{v''v''}\\ \widetilde{v''w''}\\ \widetilde{w''w''}\\ \widetilde{w''u''}\\ \varepsilon^{*}\end{bmatrix}}_{|\check{M}_n|\le1}+\underbrace{\begin{bmatrix}\bar{\rho}\tilde{V}_n\\ \bar{\rho}\tilde{V}_n\tilde{u}+\bar{p}n_x\\ \bar{\rho}\tilde{V}_n\tilde{v}+\bar{p}n_y\\ \bar{\rho}\tilde{V}_n\tilde{w}+\bar{p}n_z\\ \bar{\rho}\tilde{V}_n\check{h}_t\\ \bar{\rho}\tilde{V}_n\widetilde{u''u''}\\ \bar{\rho}\tilde{V}_n\widetilde{u''v''}\\ \bar{\rho}\tilde{V}_n\widetilde{v''v''}\\ \bar{\rho}\tilde{V}_n\widetilde{v''w''}\\ \bar{\rho}\tilde{V}_n\widetilde{w''w''}\\ \bar{\rho}\tilde{V}_n\widetilde{w''u''}\\ \bar{\rho}\tilde{V}_n\varepsilon^{*}\end{bmatrix}}_{\pm\check{M}_n>1} \tag{9}$$

where $\check{M}_n(\underline{w};n_x,n_y,n_z)=\tilde{u}_{\ell}(\underline{w})n_{\ell}\check{a}^{-1}(\underline{w})=\tilde{V}_n\check{a}^{-1}$ and $\check{a}(\underline{w})=\sqrt{[\gamma R_g\tilde{T}(\underline{w})]}$. The MUSCL variables are given by

$$\begin{aligned}\underline{w}^{\pm}_{i-\frac{1}{2},j,k}&=\underline{w}^{\pm}\Big(\underline{w}_{i-\frac{3}{2}\pm\frac{1}{2},j,k},\underline{w}_{i-\frac{1}{2}\pm\frac{1}{2},j,k},\underline{w}_{i+\frac{1}{2}\pm\frac{1}{2},j,k}\Big)\\ \underline{w}^{\pm}_{i,j-\frac{1}{2},k}&=\underline{w}^{\pm}\Big(\underline{w}_{i,j-\frac{3}{2}\pm\frac{1}{2},k},\underline{w}_{i,j-\frac{1}{2}\pm\frac{1}{2},k},\underline{w}_{i,j+\frac{1}{2}\pm\frac{1}{2},k}\Big)\\ \underline{w}^{\pm}_{i,j,k-\frac{1}{2}}&=\underline{w}^{\pm}\Big(\underline{w}_{i,j,k-\frac{3}{2}\pm\frac{1}{2}},\underline{w}_{i,j,k-\frac{1}{2}\pm\frac{1}{2}},\underline{w}_{i,j,k+\frac{1}{2}\pm\frac{1}{2}}\Big)\end{aligned} \tag{10}$$

where $\underline{w}^{\pm}$ denotes the MUSCL interpolation function. If w_p is an element of $\underline{w}=(w_p;\ p=1,\ldots,12)$, then the corresponding Van Albada limiter s_p is defined by[24]

$$s_p([w_p]_{-1},[w_p]_0,[w_p]_{+1})=\frac{2([w_p]_{+1}-[w_p]_0)([w_p]_0-[w_p]_{-1})+10^{-23}}{([w_p]_{+1}-[w_p]_0)^2+([w_p]_0-[w_p]_{-1})^2+10^{-23}}\qquad p=1,\ldots,12 \tag{11}$$

(where the 10^{-23} term is introduced to avoid division by 0) and the corresponding MUSCL variables $\underline{w}^{\pm}(\underline{w}_{-1},\underline{w}_0,\underline{w}_{+1})=(w_p^{\pm};\ p=1,\ldots,12)$ are given by[21]

$$\begin{aligned}w_p^{\pm}([w_p]_{-1},[w_p]_0,[w_p]_{+1})&=[w_p]_0\mp[(s_p/4)(1\mp s_p/3)([w_p]_{+1}-[w_p]_0)\\&\quad+(s_p/4)(1\pm s_p/3)([w_p]_0-[w_p]_{-1})]\end{aligned} \tag{12}$$

Implicit Dual Time Stepping

Denoting by $\underline{\mathcal{L}}_{i,j,k}$ the discretized form of the space operator [divergence and source terms; Eq. (6)], the semidiscrete equation at grid point (i,j,k) gives

$$\frac{\mathrm{d}\underline{w}_{i,j,k}}{\mathrm{d}t}+\underline{\mathcal{L}}_{i,j,k}\cong0\,\forall\,i,j,k\Leftrightarrow\frac{\mathrm{d}\mathfrak{w}}{\mathrm{d}t}+\boldsymbol{L}(\mathfrak{w})\cong0 \tag{13}$$

where $\mathfrak{w}=[\underline{w}_{1,1,1},\underline{w}_{1,1,2},\ldots,\underline{w}_{N_i,N_j,N_k}]^T\in\mathbb{R}^{12\times N_i\times N_j\times N_k}$ and $\boldsymbol{L}=[\underline{\mathcal{L}}_{1,1,1},\underline{\mathcal{L}}_{1,1,2},\ldots,\underline{\mathcal{L}}_{N_i,N_j,N_k}]^T\in\mathbb{R}^{12\times N_i\times N_j\times N_k}$ are the global vectors of the unknowns and of the space operators, respectively. The time discretization of the semidiscrete scheme uses a $\mathcal{O}(\Delta t)$ implicit scheme. The resulting system of nonlinear equations is solved using a dual-time-stepping iterative technique.[40] Denoting $\Delta t_{i,j,k}$ the local time step at grid point (i,j,k), $\Delta t^{*}_{i,j,k}$ the local dual pseudo time step, and defining the diagonal matrices

$$\begin{aligned}\boldsymbol{\Delta t}&=\mathrm{diag}\big[(\Delta t_{1,1,1})\underline{I}_{12},(\Delta t_{1,1,2})\underline{I}_{12},\ldots,(\Delta t_{N_i,N_j,N_k})\underline{I}_{12}\big]\\ \boldsymbol{\Delta t}^{*}&=\mathrm{diag}\big[\big(\Delta t^{*}_{1,1,1}\big)\underline{I}_{12},\big(\Delta t^{*}_{1,1,2}\big)\underline{I}_{12},\ldots,\big(\Delta t^{*}_{N_i,N_j,N_k}\big)\underline{I}_{12}\big]\end{aligned} \tag{14}$$

where $\underline{I}_{12}$ denotes the 12×12 identity matrix, the numerical scheme between instants n and $n+1$, for the dual subiteration m, can be written

$$\begin{aligned}\frac{{}^{n+1}\mathfrak{w}-{}^{n}\mathfrak{w}}{\boldsymbol{\Delta t}}+\boldsymbol{L}({}^{n+1}\mathfrak{w})\cong0\Rightarrow\frac{{}^{m+1,n+1}\mathfrak{w}-{}^{m,n+1}\mathfrak{w}}{\boldsymbol{\Delta t}^{*}}\\ +\frac{{}^{m+1,n+1}\mathfrak{w}-{}^{n}\mathfrak{w}}{\boldsymbol{\Delta t}}+\boldsymbol{L}({}^{m,n+1}\mathfrak{w})+\frac{\partial\boldsymbol{L}^{J}}{\partial\mathfrak{w}}({}^{m,n+1}\mathfrak{w})\\ \times[{}^{m+1,n+1}\mathfrak{w}-{}^{m,n+1}\mathfrak{w}]\cong0\end{aligned} \tag{15}$$

where $\boldsymbol{L}^{J}(\mathfrak{w})$ is an approximation to the operator $\boldsymbol{L}(\mathfrak{w})$, chosen so as to minimize implicit work. (The baseline choice $\boldsymbol{L}^{J}=\boldsymbol{L}$ uses the exact Jacobian in the implicit procedure.) The following iterative procedure is obtained:

Do $n_{\text{it}} = 1$, N_{it} (time steps):
Do $m_{\text{it}} = 1$, M_{it} (subiterations):

$$\left[\boldsymbol{I} + \boldsymbol{\Delta t}^{**}\frac{\partial \boldsymbol{L}^J}{\partial \mathfrak{w}}({}^{m,n+1}\mathfrak{w})\right][{}^{m+1,n+1}\mathfrak{w} - {}^{m,n+1}\mathfrak{w}]$$

$$\cong \underbrace{-\boldsymbol{\Delta t}^{**}\left[\frac{{}^{m,n+1}\mathfrak{w} - {}^{n}\mathfrak{w}}{\boldsymbol{\Delta t}} + \boldsymbol{L}({}^{m,n+1}\mathfrak{w})\right]}_{-\Delta t^{**}[{}^{m,n+1}\Re] \equiv -[{}^{m,n+1}b]} \tag{16}$$

where $\boldsymbol{I} \in \mathbb{R}^{(12\times N_i \times N_j \times N_k)\times(12\times N_i \times N_j \times N_k)}$ is the identity matrix, $\Re$ is the residual, ${}^{1,n+1}\mathfrak{w} = {}^{n}\mathfrak{w}$, and

$$\boldsymbol{\Delta t}^{**} = \frac{\boldsymbol{\Delta t}^{*}}{\boldsymbol{I} + \boldsymbol{\Delta t}^{*}/\boldsymbol{\Delta t}} \equiv [\boldsymbol{I} + \boldsymbol{\Delta t}^{-1}\boldsymbol{\Delta t}^{*}]^{-1}\boldsymbol{\Delta t}^{*} \tag{17}$$

Note that the usual non-dual-time-stepping scheme[21,25,41] is recovered at the limit $\boldsymbol{\Delta t} \to \infty \Leftrightarrow \boldsymbol{\Delta t}^{**} = \boldsymbol{\Delta t}^{*}$, with only one subiteration ($M_{\text{it}} = 1$).

Approximate Jacobians

The computational cost of the RSM method (and the corresponding overhead in comparison with more conventional two-equation closures) is basically caused by 1) the computation and assembly of the Jacobian $\partial \boldsymbol{L}^J/\partial \mathfrak{w}$ and 2) the solution of the linear system [Eq. (16)]. The following approximations were made:

1) $\mathcal{O}(\Delta x)$ Stencil: In practice, as reported in the Introduction, all authors[8,17,18] introduce a first simplification in the computation of the Jacobian $\partial \boldsymbol{L}/\partial \mathfrak{w}$ by taking the derivative of an $\mathcal{O}(\Delta x)$ stencil instead of the $\mathcal{O}(\Delta x^3)$ stencil used for the computation of the numerical fluxes [Eqs. (6), (7), and (10)]. This standard simplification, independent of the turbulence closure used, is equivalent to computing the Jacobian not from the numerical fluxes $\underline{F}^N$ but from approximate fluxes $\underline{F}^J$, where the MUSCL variables in $\underline{F}^{\pm}$ [Eq. (7)] are computed using $\mathcal{O}(\Delta x)$ extrapolation.[21–23]

2) Diagonalized viscous Jacobians: If no particular approximation of the Jacobians is made, then the computational overhead of the RSM method in comparison with two-equation closures is easily estimated because the Jacobian $\partial \boldsymbol{L}/\partial \mathfrak{w}$ is assembled from the flux Jacobians $\partial \underline{F}^N/\partial \underline{w}$ of the discretization stencil [Eq. (6)]. The size of the flux Jacobians is $12 \times 12 = 144$ for RSM computations and $7 \times 7 = 49$ for two-equation closures, and both the assembly of the Jacobian $\partial L/\partial \mathfrak{w}$ and the solution of the linear system scale as $144{:}49 = 2.93{:}1$,[12] resulting in a factor of almost three. To remove this drawback, further simplifications are made (these simplifications together with the realizability constraints are the most important result reported in the present paper) by introducing an ad hoc diagonalization of the Jacobians of the diffusive fluxes. This is done by replacing $\partial\, \underline{F}_{\ell}^{V}/\partial x_{\ell}$ by an approximate discretization of $\text{div}(\nu_{\text{eq}}\ \text{grad}\ w_p)$ for every element w_p of $\underline{w} = (w_p;\ p = 1, \ldots, 12)$ except $w_1 = \bar{\rho}$ (no diffusive fluxes in the continuity equation), where ν_{eq} is an equivalent diffusivity.[36]

3) Source terms Jacobians neglected: Computational tests[18] have indicated that including the source-term Jacobians does not seem to have a major influence on the stability of the present implicit method. Although this simplification does not result in major computational savings, it is very practical when using the computational method for turbulence model development because it does not require computing and coding source-term Jacobians for the various variants of the model.

With these simplifications the implicit operator $\partial \boldsymbol{L}/\partial \mathfrak{w}$ [Eq. (16)] is replaced by the approximate operator $\partial \boldsymbol{L}^J/\partial \mathfrak{w}$, which is the Jacobian of the approximate operator $\boldsymbol{L}^J = [\underline{\mathcal{L}}^J_{1,1,1}, \underline{\mathcal{L}}^J_{1,1,2}, \ldots, \underline{\mathcal{L}}^J_{N_i,N_j,N_k}]^T \in \mathbb{R}^{12\times N_i \times N_j \times N_k}$ obtained from

$$\underline{\mathcal{L}}^J_{i,j,k} = \frac{1}{\mathcal{V}_{i,j,k}}\begin{bmatrix} +{}^{\xi}\mathcal{S}_{i+\frac{1}{2},j,k}\ {}^{\xi}\underline{F}^J_{i+\frac{1}{2},j,k} - {}^{\xi}\mathcal{S}_{i-\frac{1}{2},j,k}\ {}^{\xi}\underline{F}^J_{i-\frac{1}{2},j,k} \\ +{}^{\eta}\mathcal{S}_{i,j+\frac{1}{2},k}\ {}^{\eta}\underline{F}^J_{i,j+\frac{1}{2},k} - {}^{\eta}\mathcal{S}_{i,j-\frac{1}{2},k}\ {}^{\eta}\underline{F}^J_{i,j-\frac{1}{2},k} \\ +{}^{\zeta}\mathcal{S}_{i,j,k+\frac{1}{2}}\ {}^{\zeta}\underline{F}^J_{i,j,k+\frac{1}{2}} - {}^{\zeta}\mathcal{S}_{i,j,k-\frac{1}{2}}\ {}^{\zeta}\underline{F}^J_{i,j,k-\frac{1}{2}} \end{bmatrix} \tag{18}$$

$${}^{\xi}\underline{F}^J_{i+\frac{1}{2},j,k} = \left[\underline{F}^{+}\left(\underline{w}_{i,j,k}; \left[{}^{\xi}n_x, {}^{\xi}n_y, {}^{\xi}n_z\right]_{i+\frac{1}{2},j,k}\right) + \underline{F}^{-}\left(\underline{w}_{i+1,j,k}; \left[{}^{\xi}n_x, {}^{\xi}n_y, {}^{\xi}n_z\right]_{i+\frac{1}{2},j,k}\right) + {}^{\xi}\underline{F}^{VJ}_{i+\frac{1}{2},j,k}\right] \tag{19}$$

$${}^{\xi}\underline{F}^{VJ}_{i+\frac{1}{2},j,k} = -\left[\underbrace{\tfrac{1}{2}([\nu_{\text{eq}}]_{i,j,k} + [\nu_{\text{eq}}]_{i+1,j,k})\frac{{}^{\xi}\mathcal{S}_{i+\frac{1}{2},j,k}}{\frac{1}{2}(\mathcal{V}_{i,j,k} + \mathcal{V}_{i+1,j,k})}}_{\mathcal{N}_{i+\frac{1}{2},j,k}}\right] \times \left\{\begin{bmatrix} 0 \\ \bar{\rho}\tilde{u} \\ \bar{\rho}\tilde{v} \\ \bar{\rho}\tilde{w} \\ \bar{\rho}\check{h}_t - \bar{p} \\ \bar{\rho}\widetilde{u''u''} \\ \bar{\rho}\widetilde{u''v''} \\ \bar{\rho}\widetilde{v''v''} \\ \bar{\rho}\widetilde{v''w''} \\ \bar{\rho}\widetilde{w''w''} \\ \bar{\rho}\widetilde{w''u''} \\ \bar{\rho}\varepsilon^{*} \end{bmatrix}_{i+1,j,k} - \begin{bmatrix} 0 \\ \bar{\rho}\tilde{u} \\ \bar{\rho}\tilde{v} \\ \bar{\rho}\tilde{w} \\ \bar{\rho}\check{h}_t - \bar{p} \\ \bar{\rho}\widetilde{u''u''} \\ \bar{\rho}\widetilde{u''v''} \\ \bar{\rho}\widetilde{v''v''} \\ \bar{\rho}\widetilde{v''w''} \\ \bar{\rho}\widetilde{w''w''} \\ \bar{\rho}\widetilde{w''u''} \\ \bar{\rho}\varepsilon^{*} \end{bmatrix}_{i,j,k}\right\} \tag{20}$$

where ν_{eq} is an equivalent diffusivity computed by MacCormack.[36] With these approximations the flux Jacobians are of the form

$$\frac{\partial {}^{\xi}\underline{F}^J_{i+\frac{1}{2},j,k}}{\partial \underline{w}_{i,j,k}} = \begin{bmatrix} {}^{\xi}\underline{\underline{A}}_{\text{MF}} & \underline{\underline{0}} \\ {}^{\xi}\underline{\underline{B}}_{\text{MF}} & {}^{\xi}\underline{\underline{A}}_{\text{RSM}} \end{bmatrix}^{i}_{i+\frac{1}{2},j,k}$$

$$\frac{\partial {}^{\xi}\underline{F}^J_{i+\frac{1}{2},j,k}}{\partial \underline{w}_{i+1,j,k}} = \begin{bmatrix} {}^{\xi}\underline{\underline{A}}_{\text{MF}} & \underline{\underline{0}} \\ {}^{\xi}\underline{\underline{B}}_{\text{MF}} & {}^{\xi}\underline{\underline{A}}_{\text{RSM}} \end{bmatrix}^{i+1}_{i+\frac{1}{2},j,k} \tag{21}$$

$$\left[{}^{\xi}\underline{\underline{A}}_{\text{RSM}}\right]^{i}_{i+\frac{1}{2},j,k} = \underbrace{\left[\frac{f^{+}_{m}(\underline{w}_{i,j,k})}{\bar{\rho}_{i,j,k}} + \mathcal{N}_{i+\frac{1}{2},j,k}\right]}_{\frac{\mathcal{V}_{i,j,k}}{{}^{\xi}\mathcal{S}_{i+\frac{1}{2},j,k}}[{}^{\xi}a]^{i}_{i+\frac{1}{2},j,k}}\underline{\underline{I}}_7$$

$$\left[{}^{\xi}\underline{\underline{A}}_{\text{RSM}}\right]^{i+1}_{i+\frac{1}{2},j,k} = \underbrace{\left[\frac{f^{-}_{m}(\underline{w}_{i+1,j,k})}{\bar{\rho}_{i+1,j,k}} - \mathcal{N}_{i+\frac{1}{2},j,k}\right]}_{\frac{\mathcal{V}_{i,j,k}}{{}^{\xi}\mathcal{S}_{i+\frac{1}{2},j,k}}[{}^{\xi}a]^{i+1}_{i+\frac{1}{2},j,k}}\underline{\underline{I}}_7$$

$$\left[{}^{\xi}\underline{\underline{A}}_{\text{RSM}}\right]^{i-1}_{i-\frac{1}{2},j,k} = \underbrace{\left[\frac{f^{+}_{m}(\underline{w}_{i-1,j,k})}{\bar{\rho}_{i-1,j,k}} + \mathcal{N}_{i-\frac{1}{2},j,k}\right]}_{-\frac{\mathcal{V}_{i,j,k}}{{}^{\xi}\mathcal{S}_{i-\frac{1}{2},j,k}}[{}^{\xi}a]^{i-1}_{i-\frac{1}{2},j,k}}\underline{\underline{I}}_7$$

$$\left[{}^{\xi}\underline{\underline{A}}_{\text{RSM}}\right]^{i}_{i-\frac{1}{2},j,k} = \underbrace{\left[\frac{f^{-}_{m}(\underline{w}_{i,j,k})}{\bar{\rho}_{i,j,k}} - \mathcal{N}_{i-\frac{1}{2},j,k}\right]}_{-\frac{\mathcal{V}_{i,j,k}}{{}^{\xi}\mathcal{S}_{i-\frac{1}{2},j,k}}[{}^{\xi}a]^{i}_{i-\frac{1}{2},j,k}}\underline{\underline{I}}_7 \tag{22}$$

where $f^{\pm}_{m}$ is the mass flux [Eq. (9)], $\mathcal{N}_{i\pm\frac{1}{2},j,k}$ is a scalar [Eq. (20)], and $\underline{\underline{I}}_7$ is the 7×7 identity matrix. The particular form of ${}^{\xi}\underline{\underline{A}}_{\text{RSM}}$ is important because it can be exploited when using approximate-factorization techniques[41] for the solution of the linear system [Eq. (16)]. Independent of the particular technique used, it is obvious that the form of the Jacobians [Eq. (21)] will result in a particular

form of the global linear system. If the vectors of unknowns are split into mean flow (MF) and turbulence (RSM) parts

$$\underline{w} = \left[\underline{w}_{\mathrm{MF}}^T, \underline{w}_{\mathrm{RSM}}^T\right]^T = \left[[\bar\rho, \bar\rho\tilde u, \bar\rho\tilde v, \bar\rho\tilde w, \bar\rho\breve h_t - \bar p];\quad [\rho\widetilde{u''u''}, \rho\widetilde{u''v''}, \rho\widetilde{v''v''}, \rho\widetilde{v''w''}, \rho\widetilde{w''w''}, \rho\widetilde{w''u''}, \rho\varepsilon^*]\right]^T$$

$$\mathfrak{w} = \left[\mathfrak{w}_{\mathrm{MF}}^T; \mathfrak{w}_{\mathrm{RSM}}^T\right]^T = \left[[(\underline{w}_{\mathrm{MF}})_{1,1,1}^T, (\underline{w}_{\mathrm{MF}})_{1,1,2}^T, \ldots, (\underline{w}_{\mathrm{MF}})_{N_i,N_j,N_k}^T];\quad [(\underline{w}_{\mathrm{RSM}})_{1,1,1}^T, (\underline{w}_{\mathrm{RSM}})_{1,1,2}^T, \ldots, (\underline{w}_{\mathrm{RSM}})_{N_i,N_j,N_k}^T]\right]^T \tag{23}$$

where $\mathfrak{w}_{\mathrm{MF}} \in \mathbb{R}^{5\times N_i\times N_j\times N_k}$ is the global vector of mean-flow variables and $\mathfrak{w}_{\mathrm{RSM}} \in \mathbb{R}^{7\times N_i\times N_j\times N_k}$ is the global vector of turbulence variables, then the global linear system [Eq. (16)] can be written as

$$\begin{bmatrix} \boldsymbol{I}_{5N_{ijk}} + \boldsymbol{A}_{\mathrm{MF}} & \boldsymbol{0} \\ \boldsymbol{B}_{\mathrm{MF}} & \boldsymbol{I}_{7N_{ijk}} + \boldsymbol{A}_{\mathrm{RSM}} \end{bmatrix} \begin{bmatrix} \Delta\mathfrak{w}_{\mathrm{MF}} \\ \Delta\mathfrak{w}_{\mathrm{RSM}} \end{bmatrix} = -\begin{bmatrix} \boldsymbol{b}_{\mathrm{MF}} \\ \boldsymbol{b}_{\mathrm{RSM}} \end{bmatrix}$$

$$\Leftrightarrow \begin{array}{l} (\boldsymbol{I}_{5N_{ijk}} + \boldsymbol{A}_{\mathrm{MF}})\Delta\mathfrak{w}_{\mathrm{MF}} = -\boldsymbol{b}_{\mathrm{MF}} \\ (\boldsymbol{I}_{7N_{ijk}} + \boldsymbol{A}_{\mathrm{RSM}})\Delta\mathfrak{w}_{\mathrm{RSM}} = -\boldsymbol{b}_{\mathrm{RSM}} - \boldsymbol{B}_{\mathrm{MF}}\Delta\mathfrak{w}_{\mathrm{MF}} \end{array} \tag{24}$$

where $\Delta\mathfrak{w} = {}^{m+1,n+1}\mathfrak{w} - {}^{m,n+1}\mathfrak{w}$ are the increments [Eq. (16)]; the matrices $\boldsymbol{A}_{\mathrm{MF}}$, $\boldsymbol{B}_{\mathrm{MF}}$, and $\boldsymbol{A}_{\mathrm{RSM}}$ are easily identified [Eqs. (16–22)]; and $\boldsymbol{b}_{\mathrm{MF}}$, $\boldsymbol{b}_{\mathrm{RSM}}$ are obtained by the splitting of $\boldsymbol{b}$ [Eq. (16)] corresponding to the splitting of $\mathfrak{w}$ [Eq. (23)]. Furthermore, a closer examination of $\boldsymbol{A}_{\mathrm{RSM}}$, as constructed by $\partial\boldsymbol{L}^J/\partial\mathfrak{w}$, and taking into account the particular form of ${}^{\xi}\underline{\underline{A}}_{\mathrm{RSM}}$, ${}^{\eta}\underline{\underline{A}}_{\mathrm{RSM}}$, ${}^{\zeta}\underline{\underline{A}}_{\mathrm{RSM}}$ [Eqs. (22)], shows that the linear system $(\boldsymbol{I}+\boldsymbol{A}_{\mathrm{RSM}})\Delta\mathfrak{w}_{\mathrm{RSM}} = -\boldsymbol{b}_{\mathrm{RSM}} - \boldsymbol{B}_{\mathrm{MF}}\Delta\mathfrak{w}_{\mathrm{MF}}$ [Eqs. (24)] is equivalent to seven independent linear systems, one for each turbulent variable v^{RSM}

$$\begin{aligned} \forall\, v^{\mathrm{RSM}} \in \{&\rho\widetilde{u''u''}, \rho\widetilde{u''v''}, \rho\widetilde{v''v''}, \rho\widetilde{v''w''}, \rho\widetilde{w''w''}, \rho\widetilde{w''u''}, \rho\varepsilon^*\} \\ &\Big\{1 + [{}^{\xi}a]^i_{i+\frac12,j,k} + [{}^{\xi}a]^i_{i-\frac12,j,k} + [{}^{\eta}a]^j_{i,j+\frac12,k} + [{}^{\eta}a]^j_{i,j-\frac12,k} \\ &+ [{}^{\zeta}a]^k_{i,j,k+\frac12} + [{}^{\zeta}a]^k_{i,j,k-\frac12}\Big\}\Delta v^{\mathrm{RSM}}_{i,j,k} + [{}^{\xi}a]^{i-1}_{i-\frac12,j,k}\Delta v^{\mathrm{RSM}}_{i-1,j,k} \\ &+ [{}^{\xi}a]^{i+1}_{i+\frac12,j,k}\Delta v^{\mathrm{RSM}}_{i+1,j,k} + [{}^{\eta}a]^{j-1}_{i,j-\frac12,k}\Delta v^{\mathrm{RSM}}_{i,j-1,k} \\ &+ [{}^{\eta}a]^{j+1}_{i,j+\frac12,k}\Delta v^{\mathrm{RSM}}_{i,j+1,k} + [{}^{\zeta}a]^{k-1}_{i,j,k-\frac12}\Delta v^{\mathrm{RSM}}_{i,j,k-1} \\ &+ [{}^{\zeta}a]^{k+1}_{i,j,k+\frac12}\Delta v^{\mathrm{RSM}}_{i,j,k+1} = -\mathfrak{B}^{\mathrm{RSM}}_{i,j,k} \end{aligned} \tag{25}$$

or equivalently

$$(\boldsymbol{I}_{N_{ijk}} + \boldsymbol{a}_{\mathrm{RSM}})\Delta\boldsymbol{v}_{\mathrm{RSM}} = -\boldsymbol{\mathfrak{B}}_{\mathrm{RSM}} \tag{26}$$

where the scalar coefficients $\{[{}^{\xi}a]^i_{i+1/2,j,k}, \ldots\}$ are easily identified [Eqs. (22)]; $\mathfrak{B}^{\mathrm{RSM}}_{i,j,k}$ is the term in $-\boldsymbol{b}_{\mathrm{RSM}} - \boldsymbol{B}_{\mathrm{MF}}\Delta\mathfrak{w}_{\mathrm{MF}}$ [Eq. (24)] corresponding to the transport equation for $v^{\mathrm{RSM}}_{i,j,k}$; $\boldsymbol{I}_{N_{ijk}}$ is the $N_{ijk}\times N_{ijk}$ identity matrix; $\boldsymbol{a}_{\mathrm{RSM}}$ is the $N_{ijk}\times N_{ijk}$ matrix assembled from the scalar coefficients $\{[{}^{\xi}a]^i_{i+1/2,j,k}, \ldots\}$ [Eq. (25)]; $\boldsymbol{v}_{\mathrm{RSM}} = [v^{\mathrm{RSM}}_{1,1,1}, v^{\mathrm{RSM}}_{1,1,2}, \ldots, v^{\mathrm{RSM}}_{N_i,N_j,N_k}]^T$; and $\boldsymbol{\mathfrak{B}}_{\mathrm{RSM}} = [\mathfrak{B}^{\mathrm{RSM}}_{1,1,1}, \mathfrak{B}^{\mathrm{RSM}}_{1,1,2}, \ldots, \mathfrak{B}^{\mathrm{RSM}}_{N_i,N_j,N_k}]^T$. This particular form can be exploited for any AF technique[41] using lower-upper (LU) decomposition[27] for the solution of the linear systems resulting from the factorization because the seven systems corresponding to the seven turbulent variables have the same system matrix (sparse $N_{ijk}\times N_{ijk}$ matrix) but different second members ($\mathfrak{B}^{\mathrm{RSM}}$), meaning that the LU decomposition needs to be computed only once. These simplifications reduce the computational effort for the matrix computation, assembly, and LU decomposition, from $12\times 12 = 144$ units to $5\times 5 + 7 = 32$ units, hence a computational economy of $\sim 144/32 = 4.5$. The same technique can be applied to two-equation closures, where the computational effort is reduced from $7\times 7 = 49$ to $5\times 5 + 2 = 27$, hence a computational economy of $\sim 49/27 = 1.81$. In this way, when using strongly implicit methods with AF techniques,[41] the ratio of computational effort for the matrix computation, assembly, and LU decomposition, between zero-equation, two-equation, and full RSM seven-equation closures scales as 25:27:32 = 1:1.08:1.28. Of course the computational effort ratio between various models also includes the computation of the residual $\mathfrak{R}$ [Eq. (16)], which scales with the number of equations, the computation of $-\boldsymbol{b}_{\mathrm{RSM}} - \boldsymbol{B}_{\mathrm{MF}}\Delta\mathfrak{w}_{\mathrm{MF}}$ [Eq. (24)], which scales with the number of turbulence variables, and the backsubstitutions after the LU decomposition, which also scale with the number of turbulence variables. This modifies the ratio of overall computation effort per subiteration between two-equation and seven-equation closures to 1:1.26 (a very substantial gain indeed compared to the initial 1:4 ratio obtained when the preceding approximations are not used[12]).

Approximate Factorization and Boundary Conditions

In the present work the linear systems appearing at every subiteration [Eqs. (24) and (26)] are solved using an approximately factored ADI–AF method[21,25]

$$\begin{aligned} &\left(\boldsymbol{I}_{5N_{ijk}} + {}^{\xi}\boldsymbol{A}_{\mathrm{MF}}\right)^{\xi}\Delta\mathfrak{w}_{\mathrm{MF}} = -\boldsymbol{b}_{\mathrm{MF}} \\ &{}^{\xi}\boldsymbol{\mathfrak{B}}_{\mathrm{RSM}} = \boldsymbol{b}_{\mathrm{RSM}} + {}^{\xi}\boldsymbol{B}_{\mathrm{MF}}{}^{\xi}\Delta\mathfrak{w}_{\mathrm{MF}} \\ &\left(\boldsymbol{I}_{N_{ijk}} + {}^{\xi}\boldsymbol{a}_{\mathrm{RSM}}\right)^{\xi}\Delta\boldsymbol{v}_{\mathrm{RSM}} = -{}^{\xi}\boldsymbol{\mathfrak{B}}_{\mathrm{RSM}} \\ &\left(\boldsymbol{I}_{5N_{ijk}} + {}^{\eta}\boldsymbol{A}_{\mathrm{MF}}\right)^{\eta}\Delta\mathfrak{w}_{\mathrm{MF}} = {}^{\xi}\Delta\mathfrak{w}_{\mathrm{MF}} \\ &{}^{\eta}\boldsymbol{\mathfrak{B}}_{\mathrm{RSM}} = -{}^{\xi}\Delta\boldsymbol{v}_{\mathrm{RSM}} + {}^{\eta}\boldsymbol{B}_{\mathrm{MF}}{}^{\eta}\Delta\mathfrak{w}_{\mathrm{MF}} \\ &\left(\boldsymbol{I}_{N_{ijk}} + {}^{\eta}\boldsymbol{a}_{\mathrm{RSM}}\right)^{\eta}\Delta\boldsymbol{v}_{\mathrm{RSM}} = -{}^{\eta}\boldsymbol{\mathfrak{B}}_{\mathrm{RSM}} \\ &\left(\boldsymbol{I}_{5N_{ijk}} + {}^{\zeta}\boldsymbol{A}_{\mathrm{MF}}\right)\Delta\mathfrak{w}_{\mathrm{MF}} = {}^{\eta}\Delta\mathfrak{w}_{\mathrm{MF}} \\ &{}^{\zeta}\boldsymbol{\mathfrak{B}}_{\mathrm{RSM}} = -{}^{\eta}\Delta\boldsymbol{v}_{\mathrm{RSM}} + {}^{\zeta}\boldsymbol{B}_{\mathrm{MF}}\Delta\mathfrak{w}_{\mathrm{MF}} \\ &\left(\boldsymbol{I}_{N_{ijk}} + {}^{\zeta}\boldsymbol{a}_{\mathrm{RSM}}\right)\Delta\boldsymbol{v}_{\mathrm{RSM}} = -{}^{\zeta}\boldsymbol{\mathfrak{B}}_{\mathrm{RSM}} \end{aligned} \tag{27}$$

for the mean flow and for the turbulence variables. The matrices ${}^{\xi}\boldsymbol{A}_{\mathrm{MF}}$, ${}^{\eta}\boldsymbol{A}_{\mathrm{MF}}$, ${}^{\zeta}\boldsymbol{A}_{\mathrm{MF}}$ (${}^{\xi}\boldsymbol{a}_{\mathrm{RSM}}$, ${}^{\eta}\boldsymbol{a}_{\mathrm{RSM}}$, ${}^{\zeta}\boldsymbol{a}_{\mathrm{RSM}}$) are obtained by retaining in $\boldsymbol{A}_{\mathrm{MF}}$ ($\boldsymbol{a}_{\mathrm{RSM}}$) only the terms corresponding to the ξ-wise, η-wise, and ζ-wise fluxes, respectively. The three successive spacewise linear systems are solved using banded-LU factorization.[27] The corresponding bandwidth is $(1 + 2\times 9)$ for the mean flow [Eqs. (27)] and only $(1 + 2)$ for the turbulence equations (27).

To achieve the high time steps used, it is indispensible to apply boundary conditions both implicitly and explicitly. Boundary conditions are treated using the method of characteristics and are treated implicitly following the corrections method of Chakravarthy,[29] applied to each linear system of the ADI–AF [Eqs. (27)].

Time Stepping

The local time step is based on a combined convective (Courant) and viscous (von Neumann) criterion[37]:

$$\Delta t_{i,j,k} \le \min\left\{\mathrm{CFL}\frac{\ell_g}{\tilde V + \breve a\sqrt{1 + \frac56(\gamma-1)M_T^2}}, \mathrm{VNN}\frac{\ell_g^2}{2\nu_{\mathrm{eq}}}\right\}$$

$$\nu_{\mathrm{eq}} = \max\left\{\frac43(\breve\nu + \nu_T), \frac{\gamma-1}{\bar\rho R_g}(\breve\kappa + \kappa_T)\right\} \tag{28}$$

where ℓ_g is the grid cell size, $\tilde V$ is the flow velocity, $\breve a$ is the sound velocity, ν_{eq} is the equivalent diffusivity computed by MacCormack,[36] $\breve\nu$ is the molecular kinematic viscosity, $\breve\kappa$ is the molecular heat

conductivity, and the eddy viscosity ν_T and eddy conductivity κ_T are those of the Launder–Sharma k–ε model[34]:

$$\nu_T = C_\mu \breve{\nu} Re_T^*, \qquad C_\mu = 0.09 \exp\left[-\frac{3.4}{\left(1+0.02Re_T^*\right)^2}\right]$$

$$Re_T^* = \frac{k^2}{\breve{\nu}\varepsilon^*}, \qquad \kappa_T = \frac{\bar{\rho}\nu_T c_p}{Pr_T}, \qquad Pr_T = 0.9 \quad (29)$$

Note that the turbulence Mach number $M_T = \sqrt{(2k\breve{a}^{-2})}$ appears in the convective stability time step.[12] When using local dual time stepping with subiterations, CFL = VNN is taken, with different values CFL and CFL* for Δt and Δt^*, respectively [Eqs. (15)].

Positivity, Boundedness, and Realizability Constraints

It is quite possible, during the iterations, to have Reynolds stresses that do not satisfy the realizability constraints introduced by Schumann.[31] Such anomalous behavior is systematically checked for at every subiteration. If the realizability constraints are not satisfied for a given grid point, then all turbulence variables are set to 0 at this grid point:

$$\text{if}\left\{\begin{array}{ccc} \widetilde{u''^2} < 0 \vee & \widetilde{v''^2} < 0 \vee & \widetilde{w''^2} < 0 \vee \\ (\widetilde{u''v''})^2 - \widetilde{u''^2}\widetilde{v''^2} > 0 \vee & (\widetilde{v''w''})^2 - \widetilde{v''^2}\widetilde{w''^2} > 0 \vee & (\widetilde{w''u''})^2 - \widetilde{w''^2}\widetilde{u''^2} > 0 \vee \\ \det[\widetilde{u_i''u_j''}] < 0 \vee & \varepsilon^* < 0 \vee & \ell_T^* = k^{\frac{3}{2}}\varepsilon^{*-1} > \ell_{T_{\max}} \end{array}\right\} : \underline{w}_{\text{RSM}} \leftarrow \underline{0} \quad (30)$$

where $\ell_{T_{\max}}$ is a maximum admissible length scale (a characteristic order-of-magnitude length of the configuration). Divisions by 0 are avoided throughout the code by adding 10^{-23} to the denominator [for every fraction $b_1/b_2 \cong b_1/(b_2 + 10^{-23})$]. These simple realizability and boundedness fixes (which are completely explicit and as a consequence easy to implement) stabilize the computations for all of the cases studied using this method.[12,15,16,20] In subsequent subiterations turbulence builds up again through diffusion from neighboring nodes.

Discussion of the Approximations

The approximate diffusive Jacobians and the fact that source-term Jacobians are neglected result, at every subiteration, in the linear system [Eq. (25)], which has the same scalar coefficients for each turbulent variable. The preceding approximation is the main reason of the computational efficiency of the method. The present approach differs substantially from the diagonal implicit algorithm of Coakley[42] because 1) the mean-flow Jacobians are not diagonalized in the present method, 2) the Reynolds-stress transport equations Jacobians are not only diagonalized but also equalized because they all correspond to the mass-flux Jacobian augmented by a diffusive contribution, and 3) the influence of the mean-flow increments on the Reynolds-stress transport equations are retained.

The particular choices for the approximate Jacobians were dictated by computational efficiency. It is well known that the inadequate implicit treatment of diffusive terms can result in numerical instabilities, especially for diffusion-dominated regions of the flowfield,[43] such as regions of large separation. Huang and Leschziner[29] and Lien and Leschziner[30] have pointed out that the absence of turbulent stresses, proportional to the mean-flow velocity gradients, in the mean-flow momentum-equations has a numerical destabilizing effect, especially in recirculating flow regions. These authors[29,30] solved the preceding stability problem by splitting the Reynolds stresses into a part proportional to the mean-flow velocity gradient (primary Boussinesq part) based on a tensorial positive eddy viscosity (defined from the corresponding Reynolds-stress transport equation) and a remaining term. The Boussinesq part was added on both sides of the momentum equation and discretized with different stencils ($\mathcal{O}[\Delta x^2]$ and $\mathcal{O}[\Delta x^4]$), thus introducing a stabilizing smoothing in the truncation error. This Boussinesq part could have been used in the approximate Jacobians [Eqs. (20)], but this was not found necessary. Instead, the LDTS subiterations served to stabilize the computations.

Finally, the explicit application of the realizability constraints and the associated fix replace the positivity-ensuring treatments of the source terms.[30–32] This particularly simple technique has given satisfactory results for a wide range of aerospace configurations considered by the authors.[12,15,16] In complex three-dimensional flow configurations[16] the Schwartz inequality constraints[31] have to be satisfied at every iteration [Eqs. (30)] to avoid the breakdown of the computational procedure.

Computational Parameters

The parameters controlling the numerical scheme (time integration) are the CFL numbers (CFL for the time step and CFL* for the dual pseudo time step, assuming that VNN = CFL and VNN* = CFL*) and the number of subiterations performed at each iteration $M_{\text{it}}(n_{\text{it}})$. This number can be either fixed by the user or chosen dynamically based on a convergence criterion for the subiterations. The relative variation of the mean flow e_{MF} and of the turbulence variables e_{RSM} are monitored using the following error L_2 pseudonorms:

$$e_{\text{MF}}[\mathfrak{w}_{\text{MF}}, \Delta\mathfrak{w}_{\text{MF}}] = \log_{10}\sqrt{\frac{1}{5}\left\{\frac{\sum[\Delta\bar{\rho}]^2}{\sum[\bar{\rho}]^2} + \frac{\sum[\Delta(\bar{\rho}\tilde{u}_i)\Delta(\bar{\rho}\tilde{u}_i)]}{\sum[\bar{\rho}\tilde{u}_i\bar{\rho}\tilde{u}_i]} + \frac{\sum[\Delta(\bar{\rho}\breve{h}_t - \bar{p})]^2}{\sum[\bar{\rho}\breve{h}_t - \bar{p}]^2}\right\}}$$

$$e_{\text{RSM}}[\mathfrak{w}_{\text{RSM}}, \Delta\mathfrak{w}_{\text{RSM}}] = \log_{10}\sqrt{\frac{1}{7}\left\{\frac{\sum[\Delta(\bar{\rho}\widetilde{u_i''u_j''})\Delta(\bar{\rho}\widetilde{u_i''u_j''})]}{\sum[\bar{\rho}\widetilde{u_i''u_j''}\bar{\rho}\widetilde{u_i''u_j''}]} + \frac{\sum[\Delta\bar{\rho}\varepsilon^*]^2}{\sum[\bar{\rho}\varepsilon^*]^2}\right\}} \quad (31)$$

where $\sum$ implies summation over all of the grid nodes and the summation convention for the Cartesian indices i, $j = 1, 2, 3$ is used [for instance, meaning that the relative variation of the momentum vector is used in Eqs. (31) for e_{MF}]. These quantities (e_{MF} and e_{RSM}) define approximately the number of digits to which the computation is converged (e.g., $e_{\text{MF}} = -4$ implies convergence to the 4.0 digit). They are used to define the subiterative convergence of the increment by the error reduction between subiterations $[m, n+1]$ and $[m+1, n+1]$ [Eqs. (16)]:

$$r_{\text{MF}}(m+1, n+1) = \log_{10}\left\{\frac{10^{[e_{\text{MF}}(m+1,n+1)]} - 10^{[e_{\text{MF}}(m,n+1)]}}{10^{[e_{\text{MF}}(m,n+1)]}}\right\}$$

$$r_{\text{RSM}}(m+1, n+1) = \log_{10}\left\{\frac{10^{[e_{\text{RSM}}(m+1,n+1)]} - 10^{[e_{\text{RSM}}(m,n+1)]}}{10^{[e_{\text{RSM}}(m,n+1)]}}\right\} \quad (32)$$

$$e_{\text{MF}}(m+1, n+1) \equiv e_{\text{MF}}\left[{}^{n}\mathfrak{w}_{\text{MF}}, {}^{m+1,n+1}\mathfrak{w}_{\text{MF}} - {}^{n}\mathfrak{w}_{\text{MF}}\right]$$

$$e_{\text{RSM}}(m+1, n+1) \equiv e_{\text{RSM}}\left[{}^{n}\mathfrak{w}_{\text{RSM}}, {}^{m+1,n+1}\mathfrak{w}_{\text{RSM}} - {}^{n}\mathfrak{w}_{\text{RSM}}\right] \quad (33)$$

The reduction (r_{MF} and r_{RSM}) indicates approximately the number of digits to which the increment is converged during the subiterations. The time-integration scheme is therefore defined by the triplet [CFL, CFL*; M_{it}, r_{MF}], where either M_{it} or r_{MF} is specified. With this nomenclature the non-LDTS scheme corresponds to [∞, CFL*; 1, $-$] [Eq. (17)].

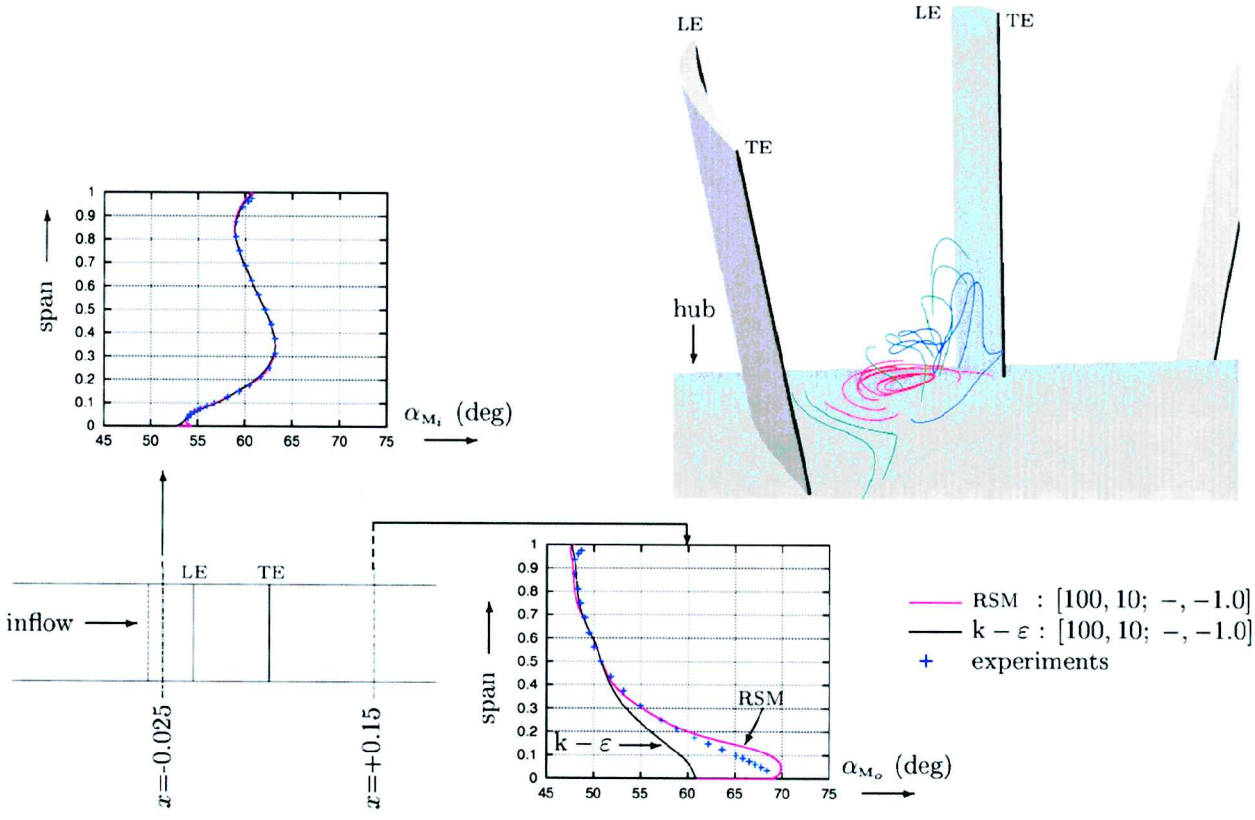

Fig. 1 Partial view of NTUA_1 annular cascade[44] with RSM-computed flow streamlines near the hub and comparison of measured and computed (using RSM[15] and $k-\varepsilon$[34] models) pitchwise-averaged flow angle at inlet α_{M_i} and outlet α_{M_o}: $\dot{m} = 13.2$ kg s^{-1}; $T_{u_i} = 4\%$; $\ell_{T_i} = 0.04$ m; and grid_DE.

Computational Results

Configurations Studied

In the following, results are presented for two different configurations chosen to highlight different aspects of the method: 1) three-dimensional flow in a subsonic annular cascade (inflow Mach number $M_i \sim 0.6$ with large hub corner stall,[44] that is used to illustrate how the subiterations solve the well-known[29,30] problem of separated flow oscillations observed with ADI–AF methods, and 2) three-dimensional flow in a transonic channel[45] with corner separation caused by shock-wave/boundary-layer interaction.

Convergence is monitored both by the evolution of global quantities such as mass flow and losses and by the error L_2 pseudonorms [Eqs. (31)] plotted as a function of either iteration count n_{it} or cummulative subiteration count:

$$\ell_{\text{it}} = m_{\text{it}} + m_{\text{it}_0}(n_{\text{it}}), \qquad m_{\text{it}_0}(n_{\text{it}}) = m_{\text{it}_0}(n_{\text{it}} - 1) + M_{\text{it}}(n_{\text{it}})$$

$$m_{\text{it}_0}(1) = 0 \tag{34}$$

For a given turbulence model the cummulative subiteration count ℓ_{it} is directly proportional to CPU time.

Importance of Subiterations

The importance of subiterations is illustrated by considering the flow in the NTUA_1 stator annular cascade,[44] which consists of 19 blades attacked by a complex swirling flow, created by an upstream scroll. Although the experiment was initially intended to investigate the effects of clearance between the blade tip and the hub, the reference case without clearance ($\delta_{\text{HTC}} = 0$) is a very interesting test case because of the experimentally observed large hub corner stall. Previous studies[16] have shown that, because of the large hub corner stall, typical two-equation closures will fail to correctly predict the substantial negative deviation (opposite to the blades' camber) of the flow near the hub (span $\varsigma = 0$–20%), whereas wall-normal free RSMs designed for separated flow[15,20] will predict this phenomenon (Fig. 1). The observed separation is basically caused by the local ($\varsigma = 0$–20%) flow incidence and has a complex three-dimensional structure (Fig. 1), consisting of a local three-dimensional tornado-type vortex (red streamlines), which is bent streamwise by the flow resulting in a strong hub-corner-stall secondary vortex (blue streamlines). This large separated flow region induces an important deflection of the flow (green streamlines) responsible for the negative deviation. A substantial improvement of outlet flow-angle prediction is obtained by the RSM closure,[15] compared to k–ε[34] results. Computations presented in the present work use an H–O–H grid of 2.75×10^6 points [grid_DE; with 129 radial stations, 25×49 (axial $\times$ tangential) points in the upstream H-grid, 241×57 (around the blade $\times$ away from blade) points in the blades-O-grid, and 97×65 (axial $\times$ tangential) points in the downstream H-grid; the nondimensional distance of the first grid point away from the wall is $n_w^+ < 0.7$ wall units everywhere], discretizing the flow around only one blade with peridocity conditions.[16] Previous published grid-convergence studies[16] using various grids, with both an RSM model[15] (which slightly overestimates separation) and the Launder–Sharma[34] k–ε (which substantially underestimates separation) indicate that results with this grid are reasonably grid converged.

The presence of the large hub corner stall promotes the numerical instabilities associated with the use of both approximate Jacobians and approximate factorization, so that typical ADI–AF schemes[12,21,25] that do not use LDTS, such as scheme [∞, 10; 1, −], will converge to a limit-cycle oscillation, which is clearly seen in the convergence of mass flow at the cascade exit $\dot{m}_o$ (Fig. 2e). With the present nomenclature the non-LDTS schemes correspond to the limit CFL $\to \infty$ [Eq. (17)], and CFL* determines the time step used. This explains why the non-DTS schemes, especially if Newton subiterations[21,25] are not performed, will be less stable than the present class of time-integration schemes with finite CFL. This is substantiated by considering various time-integration LDTS schemes (Table 2). Using the scheme [100, 10; 5, −] still exhibits limit-cycle oscillations, but with substantially diminished amplitude (Fig. 2e), and increasing the number of subiterations to 10 (scheme [100, 10; 10, −]) completely stabilizes the computations (Fig. 2e). The difference between limit-cycle and nonoscillatory convergence

is also clearly observed in the evolution of the mean-flow error e_{MF} (Fig. 2d), where the stable schemes reach a 3–4-order-of-magnitude reduction of e_{MF}, before saturation, whereas nonstable schemes fail to reduce e_{MF} by more than 1–2 orders-of-magnitude(Fig. 2d). Convergence is improved by using the [100, 10; −, −1.0] scheme that dynamically chooses the number of subiterations at each iteration to obtain a reduction $r_{MF} = -1$. In this case the number of subiterations in the initial phase of the convergence is almost constant ∼9 (Fig. 2a), but when the asymptotic phase of the convergence is reached near $\ell_{it} = 3000$ the number of subiterations M_{it} oscillates around a mean value of ∼5 (Fig. 2a), thus explaining the convergence speed-up. (It is recalled that for a given turbulence model the cumulative subiterations index ℓ_{it} is directly proportional to CPU time.) Increasing the time step will give stable computations at the expense of more subiterations and seems to increase computing time requirements, as can be seen for instance for the scheme [200, 20; −, −1.5] (Fig. 2). It is nonetheless important to note that, even for higher time steps, increasing the number of subiterations M_{it} by increasing the error reduction r_{MF} suffices to stabilize the computations (Fig. 2). As far as convergence speed is concerned, the scheme [100, 10; −, −1.0] seems optimal for the present configuration. The present configuration is however significant for testing the stability of the time-integration scheme because it contains a large region of separation and because it is computed using a quite fine grid with an RSM closure[15] that slightly overpredicts separation.

Table 2 Summary of computational parameters influence on the computations of the NTUA_1 annular, using the class of LDTS-integration schemes defined by [CFL, CFL*; M_{it}, r_{MF}] ($\dot{m} = 13.2$ kg s^{-1}; $T_{u_i} = 4\%$; $\ell_{T_i} = 0.04$ m; grid_DE)

Scheme	CFL	CFL*	M_{it}	r_{MF}	Limit cycle
Non-DTS	∞	10	1	——	Yes
DTS	100	10	5	——	Yes
DTS	100	10	10	——	No
DTS	100	10	——	−1.0	No
DTS	200	10	——	−1.0	Yes
DTS	200	10	——	−1.5	No
DTS	200	20	——	−1.5	No

Comparison of computing time requirements between the RSM and k–ε computations yields interesting and somehow unexpected conclusions (Fig. 3). Both computations were run on the same grid (grid_DE; Table 1) with the same initialization, using a [100, 10; −, −1.0] time-integration LDTS scheme. The convergence in mean-flow error e_{MF} of the k–ε computations is $\frac{1}{2}$-order-of-magnitude worse than the corresponding convergence of the RSM computations (Fig. 3b). The number of subiterations required for the k–ε computations does not drop when convergence is reached (Fig. 3a) contrary to the RSM case (Fig. 3a). Considering the convergence of mass flow at cascade exit $\dot{m}_o$ as a function of CPU time (Fig. 3c), for the two computations, indicates that, despite the 26% computational overhead per subiteration of the RSM computations, the CPU time required for full convergence is slightly higher for the k–ε computations (Fig. 3c) because more subiterations are needed for the k–ε computations (Fig. 3a). Although this result is not generally observed, it substantiates the authors' experience that, for difficult flow computations, carefully implemented RSM closures are more stable than two-equation closures, an experience contradictory with frequent assertions of the contrary.[4,5]

Transonic Nozzle Flow

The performance of the present computational method in presence of shock waves has been validated for various transonic and supersonic ($M \sim 1$–3) configurations, for which results have been presented in previous RSM closure development studies.[12,15,16,20] It is further illustrated in the present paper by considering transonic flow in a square nozzle[45] fitted with symmetric bumps on the upper and lower walls (Fig. 4), computed using a 2.03×10^6 points grid to discretize $\frac{1}{4}$ of the channel (grid_C; with $N_i \times N_j \times N_k = N_x \times N_y \times N_z = 201 \times 111 \times 91$ points, stretched geometrically away from the wall with ratios $r_j = 1.081$ and $r_k = 1.09$, respectively; the nondimensional distance of the first grid point away from the wall is $y_w^+ \cong z_w^+ < 0.5$ wall units everywhere), with y-wise and z-wise symmetry conditions. The present configuration is easier to compute (requires fewer subiterations than the preceding one), clearly indicating that numerical instabilities, caused by approximate factorization and to the approximation of the diffusive Jacobians, are mainly triggered by the presence of

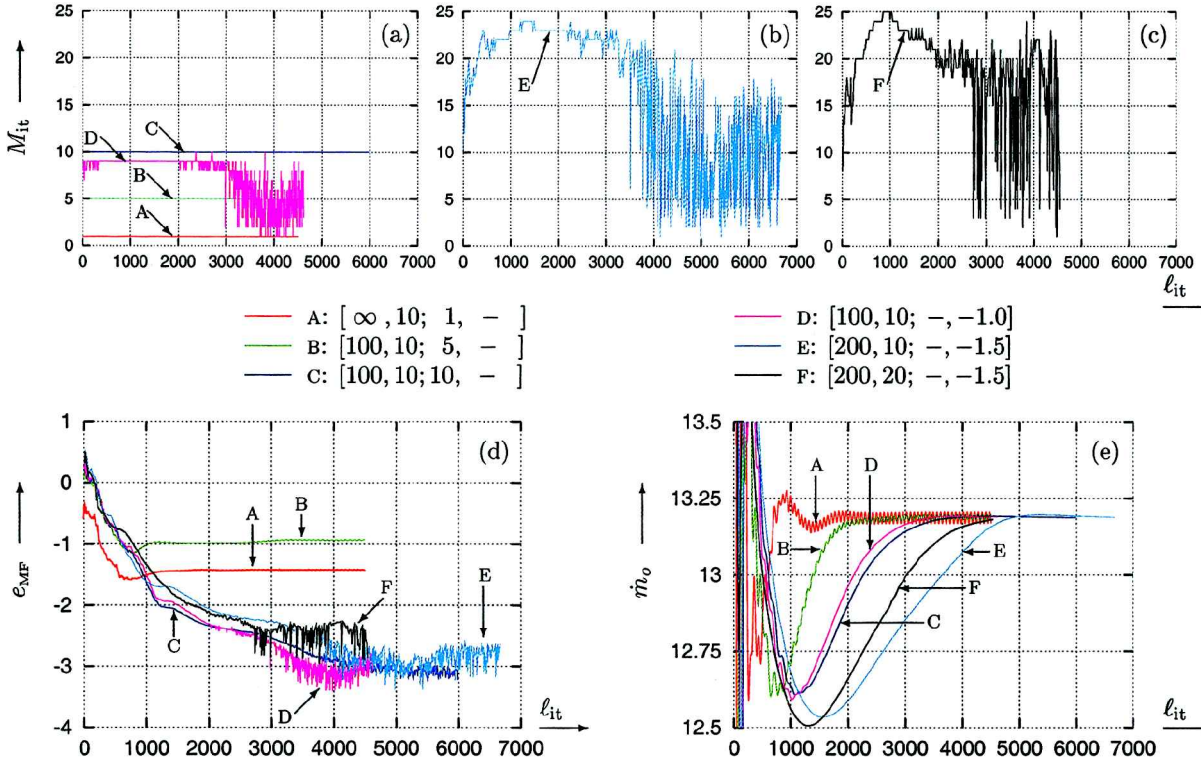

Fig. 2 Convergence of d) mean-flow error e_{MF} and e) mass flow at cascade exit $\dot{m}_o$ and a), b), and c) number of subiterations M_{it} required for a given error reduction r_{MF}, as functions of the cummulative subiteration count ℓ_{it} [Eqs. (34)], using different LDTS time-integration schemes (Table 2) for RSM[15] computations of the NTUA_1 annular cascade[44]: $\dot{m} = 13.2$ kg s^{-1}, $T_{u_i} = 4\%$, $\ell_{T_i} = 0.04$ m, and grid_DE.

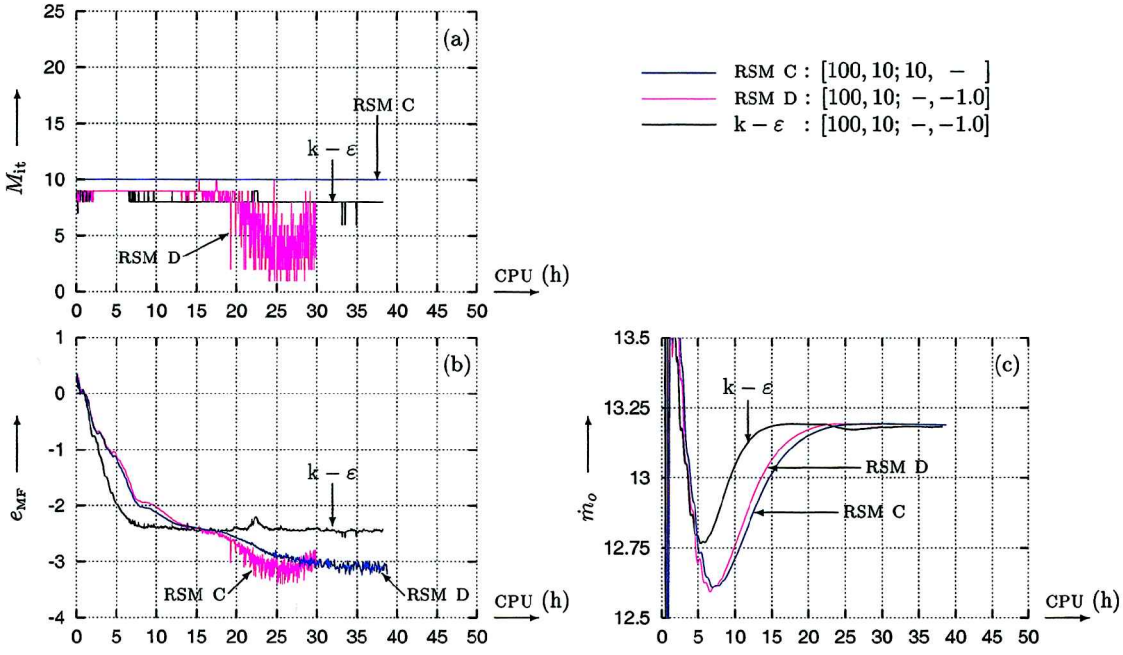

Fig. 3 Convergence of b) mean-flow error e_{MF} and c) mass flow at cascade exit $\dot{m}_o$ and a) number of subiterations M_{it} required for a given error reduction r_{MF}, as functions of CPU time (CPU hours for a 2 Gflops sustained performance), using a [100, 10; −, −1.0] time-integration LDTS scheme for RSM[15] and k–ε[34] computations of the NTUA_1 annular cascade[44]: $\dot{m} = 13.2$ kg s^{-1}, $T_{u_i} = 4\%$, $\ell_{T_i} = 0.04$ m, and grid_DE.

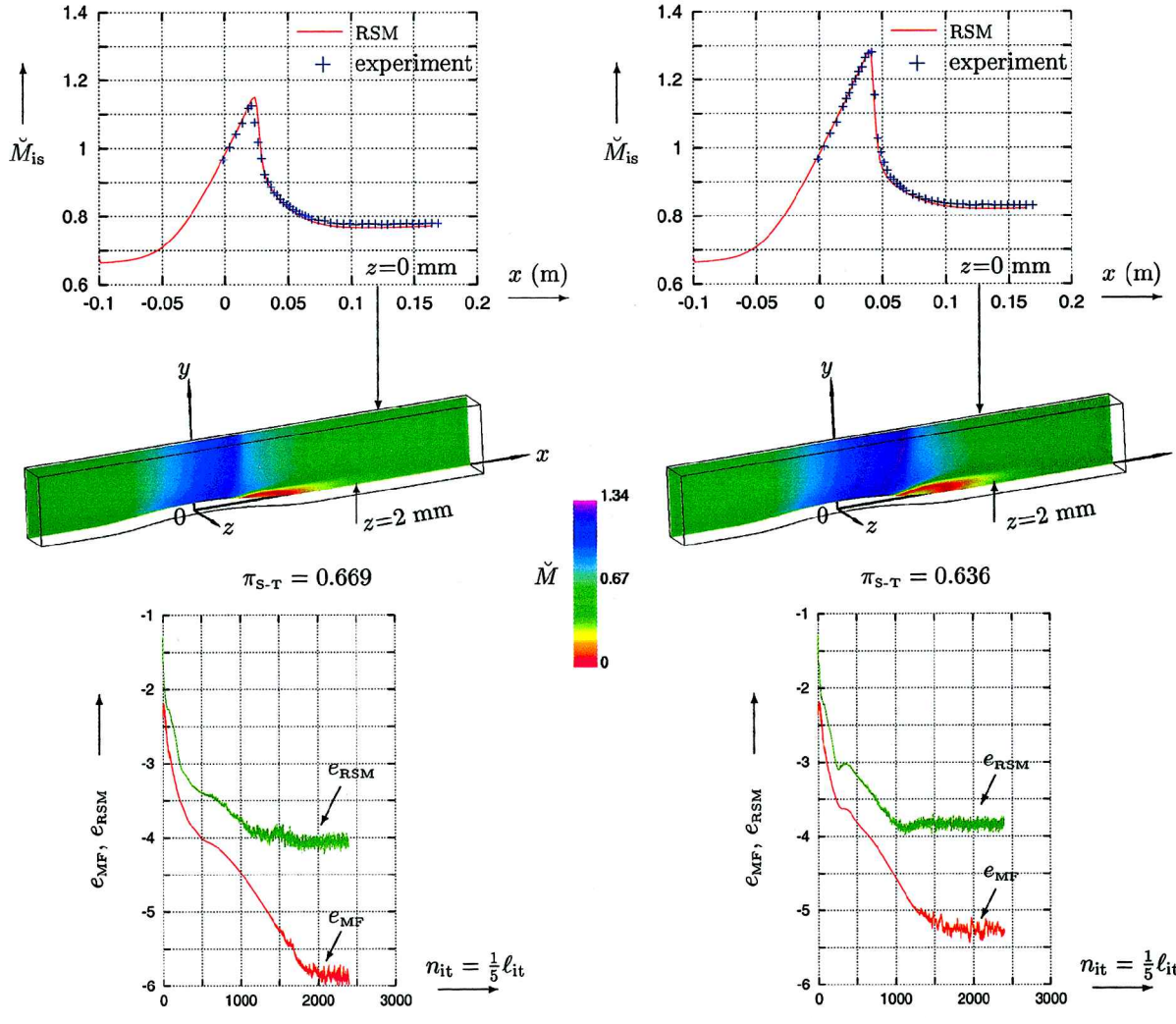

Fig. 4 Comparison of computed (using a wall-normal free version[20] of the Launder–Shima[33] RSM) and measured[45] isentropic wall Mach number $\breve{M}_{is}$, on the side wall ($z = 0$) at the y-symmetry plane of the transonic square nozzle configuration of Ott et al.[45] (only $\frac{1}{4}$ of the symmetric nozzle is shown), computed Mach-number levels near the side wall, and convergence of the computations, using a [100, 10; 5,−] time-integration scheme, for two outflow-static-to-inflow-total pressure ratios $\pi_{S\text{-}T} = 0.636, 0.669$, $T_{u_i} = 1.6\%$, $\ell_{T_i} = 0.001$ m, and 201 × 111 × 91 grid.

separated flow.[29,30] Computations were run using a [100, 10; 5, −] scheme, for two backpressure ratios (corresponding to shock-wave Mach numbers $\breve{M}_{SW}$ of 1.15 and 1.3), with the experimental inflow conditions.[46] A wall-normal free version[20] of the Launder–Shima[33] RSM (GSV-LSS) was used for these computations. The flow is strongly influenced by three-dimensional effects caused by the shock-wave/boundary-layer interaction at the solid corners because of the small width of the channel.[46] Computed wall pressures (isentropic Mach numbers[41]) show quite satisfactory agreement with measurements. The mean-flow variables error e_{MF} is reduced by 4–5 orders of magnitude before reaching saturation, whereas the turbulence variables error e_{RSM} is reduced by three orders of magnitude. This reduction is quite satisfactory, compared to the results of other authors,[13,18,14] as discussed in the Introduction of the present paper.

Conclusions

In the present work a computational methodology for the numerical integration of the Favre–Reynolds-averaged Navier–Stokes equations with near-wall RSM closure was presented and analyzed, yielding the following conclusions:

1) An implicit upwind method was used, and this seems to be the choice of all workers in the field.

2) Computational efficiency is achieved through the use of a particular form of the approximate Jacobians appearing in the implicit phase, based on an $\mathcal{O}(\Delta x)$ stencil and on approximate implicit viscous fluxes ensuring diagonalized viscous Jacobians. This form uncouples the MF equations from the RSM equations but retains the influence of the MF increments on the RSM equations. The advantage is that the implicit phase of the RSM equations corresponds to an implicit scalar approximation. In this way one subiteration using the seven-equation RSM closure is only 26% computationally more expensive than one subiteration using a two-equation closure (factor 1.26 overhead compared to a factor 3–4 overhead without approximation).

3) Computational stability loss caused by these approximations (that might result in oscillatory convergence in presence of large regions of separated flow) is compensated by using an original local-dual-time-stepping technique, with a sufficient number of subiterations, to correct the error introduced by the use of both approximate Jacobians and approximate factorization.

4) Computational robustness is ensured not only through the basic choice of an implicit upwind method but also through the use of simple explicit realizability, positivity, and boundedness fixes. No particular treatment of source terms (which were treated explicitly) was used in the present method (it was replaced by the explicit realizability constraints), but this might not be sufficient for Newton and/or multigrid methods.

5) One important conclusion of the present study is that flowfield oscillations, which are identified as physically significant large turbulent structures by several authors (the use of a full-spectrum statistical closure and a local-time-step time-nonconsistent numerical scheme notwithstanding), are more often than not an indication of limit-cycle instability of the numerical scheme. This also indicates that extreme caution should be applied, when using statistical closures in flow instabilities studies, to verify that flow oscillations are not triggered by numerical instabilities.

Possible improvements of the method are expected in 1) possible improvements in approximate factorization and implicit source-terms treatment, 2) better approximation of the equivalent diffusivity used in the approximate Jacobians for improved compatibility with the RSM closure used, and 3) convergence acceleration through the use of multigrid techniques.

It is believed that the present paper will contribute in negating the myth that near-wall low-Reynolds RSM closures suffer from inherent stabilibity problems or that they are computationally too expensive, and it is hoped that it will incite more researchers to abandon simpler (and physically less satisfactory) closures.

Acknowledgment

The computations presented in this work were run at the Institut pour le Développement des Ressources en Informatique Scientifique, where computer resources were made available by the Comité Scientifique. The authors are listed alphabetically.

References

[1]Visbal, M., and Knight, D., "The Baldwin-Lomax Turbulence Model for Two-Dimensional Shock-Wave/Boundary-Layer Interactions," *AIAA Journal*, Vol. 22, No. 7, 1984, pp. 921–928.

[2]Spalart, P. R., and Shur, M., "On the Sensitization of Turbulence Models to Rotation and Curvature," *Aerospace Sciences and Technology*, No. 5, 1997, pp. 297–302.

[3]Ekaterinaris, J. A., and Menter, F. R., "Computation of Oscillating Airfoil Flows with One- and Two-Equation Turbulence Models," *AIAA Journal*, Vol. 32, No. 12, 1994, pp. 2359–2365.

[4]Barakos, G., and Drikakis, D., "Investigation of Nonlinear Eddy-Viscosity Turbulence Models in Shock/Boundary-Layer Interaction," *AIAA Journal*, Vol. 38, No. 3, 2000, pp. 461–469.

[5]Rumsey, C. L., Gatski, T. B., and Morrison, J. H., "Turbulence Model Predictions of Strongly Curved Flow in a U-Duct," *AIAA Journal*, Vol. 38, No. 8, 2000, pp. 1394–1402.

[6]Hah, C., "Calculation of Three-Dimensional Viscous Flows in Turbomachinery with an Implicit Relaxation Method," *Journal of Propulsion and Power*, Vol. 3, No. 5, 1987, pp. 415–422.

[7]Lin, H., Yang, D. Y., and Chieng, C. C., "Variants of Biconjugate-Gradient Method for Compressible Navier–Stokes Solver," *AIAA Journal*, Vol. 33, No. 7, 1995, pp. 1177–1184.

[8]Batten, P., Leschziner, M. A., and Goldberg, U. C., "Average-State Jacobians and Implicit Methods for Compressible Viscous and Turbulent Flows," *Journal of Computational Physics*, Vol. 137, 1997, pp. 38–78.

[9]Gerlinger, P., and Brüggemann, D., "An Implicit Multigrid Scheme for the Compressible Navier–Stokes Equations with Low-Reynolds-Number Turbulence Closure," *Journal of Fluids Engineering*, Vol. 120, 1998, pp. 257–262.

[10]Gatski, T. B., and Speziale, C. G., "On Explicit Algebraic Stress Models for Complex Turbulent Flows," *Journal of Fluid Mechanics*, Vol. 254, 1993, pp. 59–78.

[11]Sotiropoulos, F., and Patel, V. C., "Application of Reynolds-Stress Transport Models to Stern and Wake Flows," *Journal of Ship Research*, Vol. 39, No. 4, 1995, pp. 263–283.

[12]Gerolymos, G. A., and Vallet, I., "Near-Wall Reynolds-Stress Three-Dimensional Transonic Flow Computation," *AIAA Journal*, Vol. 35, No. 2, 1997, pp. 228–236.

[13]Chenault, C. F., Beran, P. S., and Bowersox, R. D. W., "Numerical Investigation of Supersonic Injection Using a Reynolds-Stress Turbulence Model," *AIAA Journal*, Vol. 37, No. 10, 1999, pp. 1257–1269.

[14]Batten, P., Craft, T. J., Leschziner, M. A., and Loyau, H., "Reynolds-Stress-Transport Modeling for Compressible Aerodynamics Applications," *AIAA Journal*, Vol. 37, No. 7, 1999, pp. 785–797.

[15]Gerolymos, G. A., and Vallet, I., "Wall-Normal-Free Near-Wall Reynolds-Stress Closure for Three-Dimensional Compressible Separated Flows," *AIAA Journal*, Vol. 39, No. 10, 2001, pp. 1833–1842.

[16]Gerolymos, G. A., Neubauer, J., Sharma, V. C., and Vallet, I., "Improved Prediction of Turbomachinery Flows Using Near-Wall Reynolds-Stress Model," *Journal of Turbomachinary*, Vol. 124, 2002, pp. 86–99.

[17]Morrison, J. H., "A Compressible Navier–Stokes Solver with 2-Equation and Reynolds-Stress Turbulence Closure Models," NASA CR 4440, Oct. 1992; also AIAA Paper 90-5251, May 1990.

[18]Vallet, I., "Aérodynamique Numérique 3-D Instationnaire avec Fermeture Bas-Reynolds au Second Ordre," Ph.D. Dissertation, Univ. Pierre-et-Marie-Curie, Paris, Dec. 1995.

[19]Zhang, H. S., So, R. M. C., Gatski, and Speziale, C. G., "A Near-Wall Second-Order Closure for Compressible Turbulent Flows," *Near-Wall Turbulent Flows*, edited by R. M. C. So, C. G. Speziale, and B. E. Launder, Elsevier, New York, 1993, pp. 209–218.

[20]Gerolymos, G. A., and Vallet, I., "Advanced Turbulence Modelling for Transonic Shock-Wave/Boundary-Layer Interaction," *Symposium Transsonicum IV*, 2002, Göttingen [D]; also "Computation of 3-D Aerospace Configurations Using Wall-Normal-Free Reynolds-Stress Models," *International Journal Heat of Fluid Flow* (submitted for publication).

[21]Anderson, W. K., Thomas, J. L., and Van Leer, B., "Comparison of Finite-Volume Flux-Vector-Splittings for the Euler Equations," *AIAA Journal*, Vol. 24, No. 9, 1986, pp. 1453–1460.

[22]Toro, E. F., *Riemann Solvers and Numerical Methods for Fluid Dynamics*, Springer-Verlag, Berlin, 1997, pp. 293–308, 313–341, 422–458.

[23]Hirsch, Ch., *Numerical Computation of Internal and External Flows II*, Wiley, New York, 1991, pp. 362–366, 460–469, 536–556.

[24]Venkatakrishnan, V., "Preconditioned Conjugate Gradient Methods for the Compressible Navier–Stokes Equations," *AIAA Journal*, Vol. 29, No. 7, 1991, pp. 1092–1100.

[25]Anderson, W. K., Thomas, J. L., and Rumsey, C. L., "Extension and Application of Flux-Vector-Splitting to Calculations on Dynamic Meshes," *AIAA Journal*, Vol. 27, No. 6, 1989, pp. 673, 674; also AIAA Paper 87-1152, June 1987.

[26]Arnone, A., "Viscous Analysis of 3-D Rotor Flow Using a Multigrid Method," *Journal of Turbomachinery*, Vol. 116, 1994, pp. 435–445.

[27]Golub, G. H., and Van Loan, C. F., *Matrix Computations*, Johns Hopkins Univ. Press, Baltimore, MD, 1989, pp. 150–152.

[28]Chakravarthy, S. R., "Relaxation Methods for Unfactored Implicit Upwind Schemes," AIAA Paper 84-0165, Jan. 1984.

[29]Huang, P. G., and Leschziner, M. A., "Stabilization of Recirculating Flow Computations Performed with Second Moment Closure and 3-Order Discretization," *Proceedings of the 5th Turbulent Shear Flows*, Cornell Univ., Ithaca, NY, 1985, pp. 20·7–20·12.

[30]Lien, F. S., and Leschziner, M. A., "Second Moment Closure for 3-D Turbulent Flow Around and Within Complex Geometries," *Computers and Fluids Journal*, Vol. 25, 1996, pp. 237–262.

[31]Schumann, U., "Realizability of Reynolds-Stress Turbulence Models," *Physics of Fluids*, Vol. 20, 1977, pp. 721–725.

[32]Pantakar, S. V., *Numerical Heat Transfer and Fluid Flow*, Hemisphere, Washington, DC, 1980, pp. 36–39, 48, 49, 143–146.

[33]Launder, B. E., and Shima, N., "2-Moment Closure for the near-Wall Sublayer: Development and Application," *AIAA Journal*, Vol. 27, No. 10, 1989, pp. 1319–1325.

[34]Launder, B. E., and Sharma, B. I., "Application of the Energy Dissipation Model of Turbulence to the Calculation of Flows near a Spinning Disk," *Letters in Heat and Mass Transfer*, Vol. 1, 1974, pp. 131–138.

[35]Craft, T. J., and Launder, B., "A Reynolds-Stress Model Designed for Complex Geometries," *International Journal of Heat Fluid Flow*, Vol. 17, 1996, pp. 245–254.

[36]MacCormack, R. W., "A Numerical Method for Solving the Equations of Compressible Viscous Flow," *AIAA Journal*, Vol. 20, No. 9, 1982, pp. 1275–1281.

[37]Kunz, R. F., and Lakshminarayana, B., "Stability of Explicit Navier–Stokes Procedures Using k–ε and k–ε/Algebraic Reynolds Stress Turbulence Models," *Journal of Computational Physics*, Vol. 103, 1992, pp. 141–159.

[38]Morrison, J. H., Gatski, T. B., Sommer, T. P., Zhang, H. S., and So, R. M. C., "Evaluation of a near-Wall Turbulent Closure Model in Predicting Compressible Ramp Flows," *Near-Wall Turbulent Flows*, edited by R. M. C. So, C. G. Speziale, and B. E. Launder, Elsevier, New York, 1993, pp. 239–250.

[39]Chenault, C. F., and Beran, P. S., "K–ϵ and Reynolds Stress Turbulence Model Comparisons for Two-Dimensional Injection Flows," *AIAA Journal*, Vol. 36, No. 8, 1998, pp. 1401–1412.

[40]Dubuc, L., Cantariti, F., Woodgate, M., Gribben, B., Badcock, K. J., and Richards, B. E., "Solution of the Unsteady Euler Equations Using an Implicit Dual-Time Method," *AIAA Journal*, Vol. 36, No. 8, 1998, pp. 1417–1424.

[41]Mottura, L., Vigevano, L., and Zaccanti, M., "Factorized Implicit Upwind Methods Applied to Inviscid Flows at High Mach Number," *AIAA Journal*, Vol. 38, No. 10, 2000, pp. 1846–1852.

[42]Coakley, T. J., "Implicit Upwind Methods for the Compressible Navier–Stokes Equations," *AIAA Journal*, Vol. 23, No. 3, 1985, pp. 374–380; also NASA TM 85899, Feb. 1984.

[43]Shih, T. I. P., Steinthorsson, E., and Chyu, W. J., "Implicit Treatment of Diffusion Terms in Lower-Upper Algorithms," *AIAA Journal*, Vol. 31, No. 4, 1993, pp. 788–791.

[44]Doukelis, A., Mathioudakis, K., and Papailiou, K., "The Effect of Tip Clearance Gap Size and Wall Rotation on the Performance of a High-Speed Annular Compressor Cascade," American Society of Mechanical Engineers, Paper 98-GT-38, June 1998.

[45]Ott, P., Bölcs, A., and Fransson, T. H., "Experimental and Numerical Study of the Time-Dependent Pressure Response of a Shock-Wave Oscillating in a Nozzle," *Journal of Turbomachinery*, Vol. 117, 1995, pp. 106–114.

[46]Gerolymos, G. A., Vallet, I., Ott, P., and Bölcs, A., "Computation of Unsteady Transonic Nozzle Flows Using k–ε Turbulence Closure," *AIAA Journal*, Vol. 34, No. 7, 1996, pp. 1331–1340.

R. M. C. So
Associate Editor

Color reproductions courtesy of Université Pierre-et-Marie-Curie.